Article

Use of Kane's Method for Multi-Body Dynamic Modelling and Control of Spar-Type Floating Offshore Wind Turbines

Saptarshi Sarkar [1] and **Breiffni Fitzgerald** [2,*]

1   Department of Mechanics and Maritime Sciences, Chalmers University of Technology,
    412 96 Gothenburg, Sweden; ssarkar@chalmers.se
2   School of Engineering, Trinity College, Dublin 2, Ireland
*   Correspondence: breiffni.fitzgerald@tcd.ie

Abstract: This paper demonstrates the use of Kane's method to derive equations of motion for a spar-type floating offshore wind turbine taking into account the flexibility of the members. The recently emerged Kane's method reduces the effort required to derive equations of motion for complex multi-body systems, making them simpler to model and more readily solved by computers. Further, the installation procedure of external vibration control devices on the wind turbine using Kane's method is described, and the ease of using this method has been demonstrated. A tuned mass damper inerter (TMDI) is installed in the tower for illustration. The excellent vibration mitigation properties of the TMDI are also presented in this paper.

Keywords: flexible multi-body dynamics; Kane's method; floating offshore wind turbines; control; tuned mass damper inerter

1. Introduction

The rapid expansion of global wind energy capacity from 59.1 gigawatts (GW) [1] in 2005 to 743 GW [2] in 2021 has been mainly due to developments in wind turbine technology during this period. With the increasing demand for renewable energy, researchers have worked actively to study the dynamic behavior of wind turbines. These structures have now grown to be the largest rotating structures on Earth. It is not uncommon to have tower heights greater than 100 m and blade lengths exceeding 80 m. Indeed the current trends indicate that these components will continue to increase in size for the foreseeable future. The increase in the size of wind turbine components has led to increased flexibility and dynamic structural effects that cannot be ignored in design. The harsh environment that these structures are necessarily placed in further complicates matters. Offshore wind turbines are subjected to large magnitude turbulent aerodynamic loading and hydrodynamic loads from waves and current. Floating offshore wind turbines (FOWTs) have recently been proposed and developed, and these structures are inherently more dynamic than traditional fixed-base offshore wind turbines. With bigger structural components and floating support structures, the general assumptions made by most design codes of small deflections and the application of loads on the undeformed structure do not hold. As a result, modeling of FOWTs has become an increasingly important area of research in the wind turbine industry. These models have been used for structural control and health monitoring, fatigue analysis, optimised design, etc. Much work has taken place in this area in the last decade.

Many researchers have developed dynamic models based on the Euler–Lagrange energy formulation approach. One of the earliest such models was developed by Murtagh et al. [3] for onshore wind turbines. The dynamics of onshore wind turbines have been extensively studied using Euler–Lagrange models for applications such as structural control [4–10], structural health monitoring [11,12], soil-structure interaction [13–17], etc. Euler–Lagrange models have also been used to model offshore wind turbines. Dinh et al. [18]

developed FOWT models with a view to vibration control of their structural components. Lackner [19,20] also developed FOWT models for use in structural control applications. The dynamics of FOWTs were also studied in several works [21–24]. Dynamics of spar-type offshore wind turbines were studied in Karimirad and Moan [21,23]. Waris et al. [22] studied the dynamics of offshore wind turbines with different kinds of heave plates and mooring systems.

Multi-body dynamic models have also been developed for offshore wind turbines. FAST [25,26], an open-source wind turbine simulation tool developed by the National Renewable Energy Laboratory (NREL) in the United States, is one of the most popular tools used to simulate the dynamic behaviour of wind turbines. FAST models the wind turbine as a multi-body system using Kane's method [27] similar to the works in [28–33]. Similar to FAST, HAWC2 [34] was developed in the Technical University of Denmark, Risø to study the dynamics of horizontal axis wind turbines. Numerical codes such as FAST, HAWC2, the one developed in this paper, etc., can be further validated against experimental results. One such database of test cases is provided in [35]. Although models such as FAST and HAWC2 have been developed, little publication on the formulation FOWTs is available. It is not easy to find detailed work describing the formulation of the FOWT equations of motion and subsequent dynamic analysis in the published literature.

The literature reviewed in this section summarises the different approaches that researchers have used for the dynamic modeling of flexible multi-body wind turbines and their foundations, ranging from simple lumped mass models to sophisticated finite element models. Much work has been done in the field of FOWT dynamics. However, literature is unavailable on the formulation and modeling of FOWTs using the recently emerged Kane's method. Therefore, the scope of this paper is enlisted as follows.

1. The paper demonstrates in detail the use of the recently emerged Kane's method in deriving the equations of motion of flexible multi-body systems like FOWTs. The method presented here is general and applies to any wind turbine or mechanical system. Such detailed discussion on Kane's method for flexible multi-body modeling is unavailable in the literature.
2. The paper details the powerful vector approach brought about by Kane's method, which allows the formulation of the dynamics of the complex wind turbine system relatively easy.
3. The paper further demonstrates the installation method of an external damper in the FOWT using Kane's method. The purpose of this exercise is to emphasize the ease of using Kane's method in augmenting/coupling the system equations with an auxiliary device. Again, the steps presented here are general and apply to any auxiliary device.

Modern-day wind turbines are a combination of large flexible components which undergo large deformations and rigid bodies. The various parts of the wind turbine come together to extract kinetic energy from the inflow wind. The blades of a multi-megawatt wind turbine are mounted on the hub at the tip of the low-speed shaft. The shaft is often tilted up, and the blades are coned to avoid tower strikes during operation. The conversion of mechanical torque to electrical power has quite a few stages and involves many components. Modeling such a wind turbine requires a detailed multi-body approach. A multi-body approach consists primarily of provisions made to accommodate the fact that reference frames play a central role in connection with many of the vectors of interest that determine the dynamics of the wind turbine system. Every component of the wind turbine must be defined in its own coordinate system/reference frames. The inclusion of multiple coordinate systems to model various components of a system limits the use of classical methods (like energy methods) in deriving equations of motion. A vector approach is hence required to replace the classical scalar approaches. Kane's method has been shown to reduce the effort required to derive equations of motion for complex multi-body systems, making them simpler to model and more readily solved by computers. In this study, Kane's method [27] is used to derive the dynamic equations of a flexible wind turbine. Throughout the study, bold upper case letters are used for matrices, and bold lower case letters are used for vectors.

2. Methodology

This section presents the development of the flexible multi-body dynamic model for the FOWTs. In the following sections, the assumptions made to facilitate the development of the equations of motion are presented first. The following sections present the kinematics and kinetics of the system. Then, the dynamic loads on the turbine are described briefly. This section concludes with a discussion on structural control of wind turbine towers using passive tuned mass inerter dampers (TMDIs).

2.1. Assumptions

The wind turbine is modelled as a flexible multi-body dynamical system. The various components of importance are the tower, the nacelle, the generator, the gearbox, the low-speed shaft, the hub, and the blades. The tower, the blades, and the low-speed shaft are the flexible components of the wind turbine. Modal analysis is often used to study the dynamics of flexible members. The tower is modelled using the first and second modes in fore-aft and side-to-side directions. Futhermore, the first two modes in flapwise and the first mode in edgewise directions are used for the blades. It is assumed that since the members are highly flexible, the first few modes will capture the dynamics with sufficient accuracy [36]. The degrees of freedom that define the motion of a floating offshore wind turbine are the platform motions, the tower vibrations, the nacelle yaw motion, the torsional distortion of the low-speed shaft, the generator azimuth angle, and the elastic deflections of the three blades. Therefore, the degrees of freedom for a three-bladed wind turbine can be written as

$$\boldsymbol{q} = [q_{Sg} \; q_{Sw} \; q_{Hv} \; q_R \; q_P \; q_Y \; q_{TFA1} \; q_{TSS1} \; q_{TFA2} \; q_{TSS2} \; q_{yaw} \; q_{GeAz} \; q_{DrTr} \cdots \\ \cdots \; q_{B1F1} \; q_{B1E1} \; q_{B1F2} \; q_{B2F1} \; q_{B2E1} \; q_{B2F2} \; q_{B3F1} \; q_{B3E1} \; q_{B3F2}]^T \tag{1}$$

Therefore, a 22 degrees of freedom model will be derived to model the wind turbine. The degrees of freedom are also denoted by numbers 1 to 22 in the same sequence as presented in Equation (1). The degrees of freedom are schematically shown in Figure 1. A list of the DOFs is presented in Appendix A. Throughout the study, the name of the DOF and its corresponding number will be used interchangeably. Coordinate systems will be assigned to each component, and the motion in its local reference frame will be transformed to the global/inertial reference frame. In the following sections, the coordinate systems required for the wind turbine will be defined, followed by the system's kinematics and, finally, the system's kinetics, which will be used to derive the equations of motion.
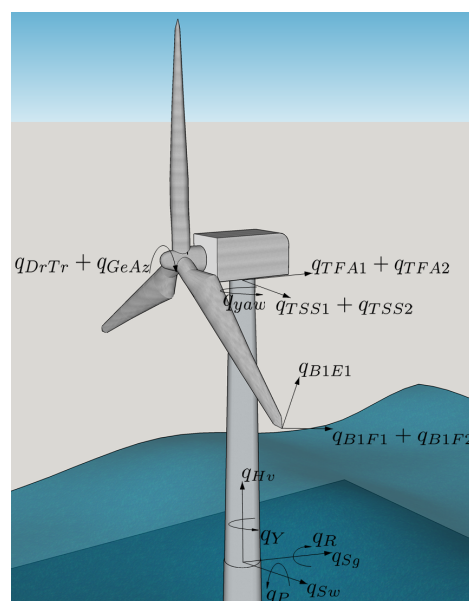

Figure 1. Schematic diagram of the degrees of freedom.

2.2. Coordinate Systems

As mentioned earlier, individual components of the floating offshore wind turbine are modelled in their local reference frames. A combination of small angle approximation (small angle rotation) and Euler angles (Euler rotation) are used to establish transformation relations between the coordinate systems. Three consecutive rotations θ_1, θ_2 and θ_3 about three mutually orthogonal axes $(\hat{X}_1, \hat{X}_2, \hat{X}_3)$ result in a set of orthogonal axes $(\hat{x}_1, \hat{x}_2, \hat{x}_3)$. This transformation with small angle approximation can be defined as

$$
\begin{pmatrix} \hat{x}_1 \\ \hat{x}_2 \\ \hat{x}_3 \end{pmatrix} \approx \underbrace{\begin{bmatrix} 1 & \theta_3 & -\theta_2 \\ -\theta_3 & 1 & \theta_1 \\ \theta_2 & -\theta_1 & 1 \end{bmatrix}}_{T} \begin{pmatrix} \hat{X}_1 \\ \hat{X}_2 \\ \hat{X}_3 \end{pmatrix}
\tag{2}
$$

The small angle approximation makes the transformation independent of the order of rotation. Here, the approximation sign is used since the transformation matrix T is not orthonormal and hence the resulting set of axes are not orthogonal to each other. The nearest orthonormal matrix is hence obtained by Singular Value Decomposition (SVD). The nearest orthonormal matrix in Frobenius norm sense T_O is given as

$$
T_O = UV'
\tag{3}
$$

where the columns of U contain the eigenvectors of TT' and the columns of V contain eigenvectors of $T'T$. This follows from the result of SVD of T obtained as

$$
T = U\Sigma V'
\tag{4}
$$

where Σ is a diagonal matrix containing the singular values of T. Σ can be obtained as

$$
\Sigma = \sqrt{\text{eigenvalues of } TT'} = \sqrt{\text{eigenvalues of } T'T}
\tag{5}
$$

The matrix $T_O(\theta_1, \theta_2, \theta_3)$ will be used to define transformations about three mutually perpendicular axes $(\hat{X}_1, \hat{X}_2, \hat{X}_3)$ when small angle approximation is employed. The different coordinate systems used are defined as follows.

To accurately model a multi-body system like an offshore wind turbine, the kinematics of each sub-component of the wind turbine is first written in its local reference frame and then referred back to the inertial (global) reference frame denoted by $\hat{z}$. Figure 2 shows the different reference frames used in this paper. As shown in Figure 2, local coordinate systems/reference frames are attached to the floating platform $(\hat{a})$, tower nodes along the height of the tower, the tower-top $(\hat{b})$, the nacelle $(\hat{d})$, non-rotating reference frame attached to the low-speed shaft $(\hat{c})$ and rotating reference frame $(\hat{e})$ of the rotor and the blades $(\hat{g})$. To accurately model the blades, they are first coned $(\hat{i})$ then pitched (not pictured in Figure 2). Node-fixed coordinate systems are defined on the blades which are further rotated according to the elastic deflection of the blades in out-of-plane and in-plane directions. These blade node-fixed reference frames are used to estimate and return aerodynamic loads. The platform and the blades and the tower deforms/rotates simultaneously about more than one axis. Therefore, Euler rotation matrix cannot be used to define the transformation between two reference frames. However, as the magnitude of these angles is relatively small, the approximation derived in Equation (3) is used. All coordinate systems used in this paper are described in details in Appendix B.
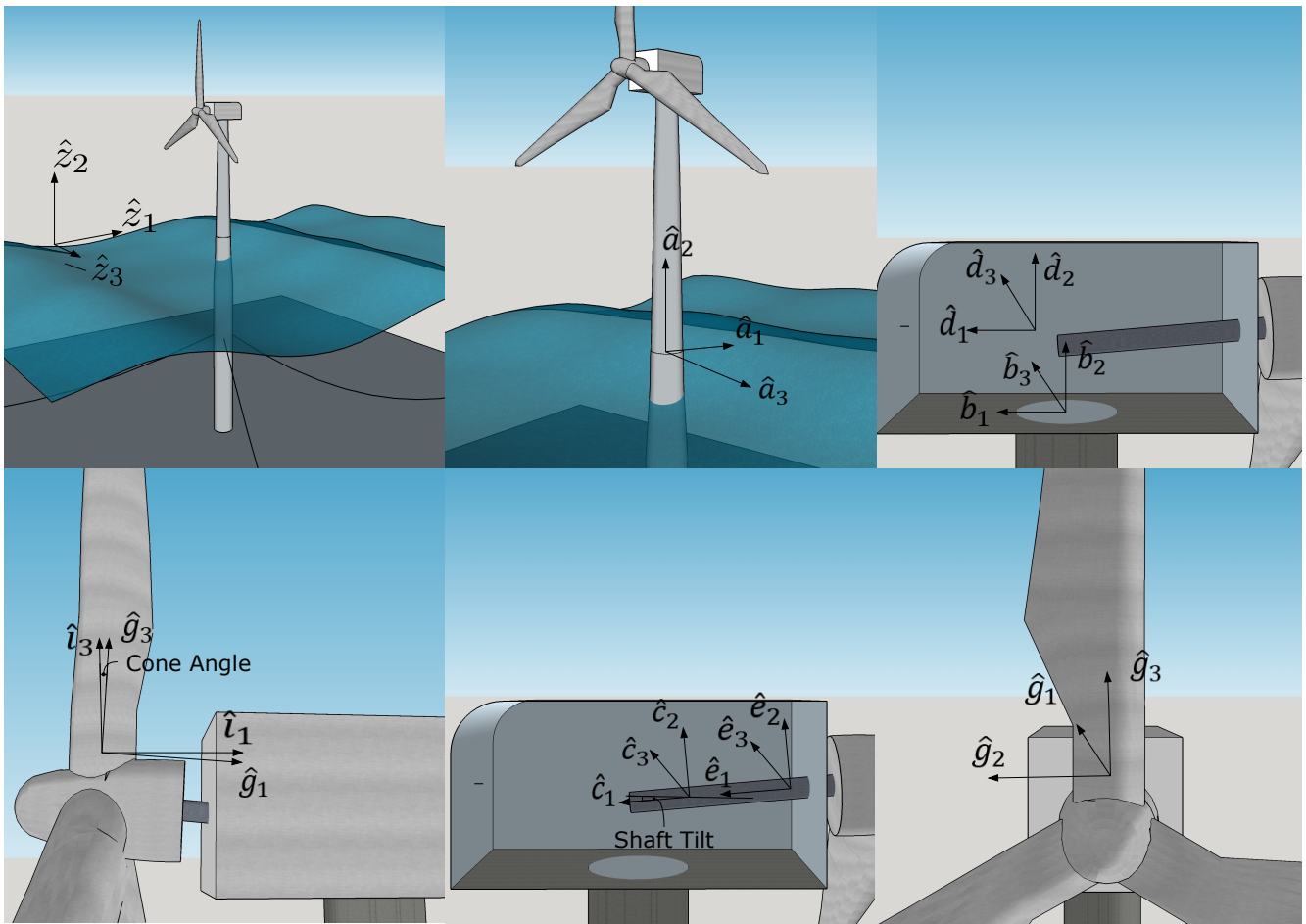
Figure 2. Coordinate systems for Spar Type FOWT [30].

2.3. Kinematics

With all the required coordinate systems on the FOWT defined, the next step is to define the kinematics of the FOWT. For that, first important points on the turbine are identified that describe the kinematics of the entire system. The important points that describe the motion are as follows: Z (tower-base), T (tower node), O (tower-top/base-plate/yaw bearing mass centre), U (nacelle centre of mass), Q (apex of conning angle), C (hub centre of mass), S1 (blade nodes for blade 1), S2 (blade nodes for blade 2) and S3 (blade nodes for blade 3). The various reference frames of importance are denoted as: E (earth/inertial), X (tower base), F (tower body element), B (tower-top/base-plate), N (nacelle), L (low speed shaft on rotor end), M1 (blade 1 element body), M2 (blade 2 element body), M3 (blade 3 element body) and G (high speed shaft/generator).

The complete kinematic description involves defining the position, velocity and acceleration of each rigid and flexible member of the turbine. For brevity, all equations are presented in Appendix B. With the kinematics of the system defined, the kinetics and equations of the motion of the FOWT can be derived as presented in the next section.

2.4. Kinetics and Kane's Equation of Motion

In this section, the equations of motion of a 3-bladed floating offshore wind turbine will be derived. As per [27], Kane's equations of motion for a holonomic system with 22 DOFs are stated as

$$F_r + F_r^* = 0 \quad \text{for } r = 1 \text{ to } 22 \tag{6}$$

where F_r and F_r^* are the generalised active and the generalised inertia forces respectively. In a set of n rigid bodies characterised by reference frame N_i and centre of mass point X_i

the generalised active and inertial forces are given as

$$F_r = \sum_{i=1}^{n} {}^{E}v_r^{X_i} \cdot \mathbf{F}^i + {}^{E}\omega_r^{N_i} \cdot \mathbf{M}^{N_i} \quad \text{for } r = 1 \text{ to } 22$$

$$F_r^* = -\sum_{i=1}^{n} {}^{E}v_r^{X_i} \cdot \left(m^{N_i E} a^{X_i} \right) - {}^{E}\omega_r^{N_i} \cdot {}^{E}\dot{H}^{N_i} \quad \text{for } r = 1 \text{ to } 22 \tag{7}$$

At every rigid body N_i, the active forces are applied at the centre of mass X_i. The time derivative of the angular momentum of rigid body N_i about its centre of mass X_i is obtained as [27]

$$^{E}\dot{H}^{N_i} = \bar{\bar{I}}^{N_i} \cdot {}^{E}\alpha^{N_i} + {}^{E}\omega^{N_i} \times \bar{\bar{I}}^{N_i} \cdot {}^{E}\omega^{N_i} \tag{8}$$

The mass of the platform, the tower, the yaw bearing, the nacelle, the hub, the blades and the generator contribute to the total generalised inertia force

$$F_r^* = F_r^*\big|_X + F_r^*\big|_T + F_r^*\big|_N + F_r^*\big|_H + F_r^*\big|_{B1} + F_r^*\big|_{B2} + F_r^*\big|_{B3} + F_r^*\big|_G \tag{9}$$

Generalised active forces are the forces applied directly on the wind turbine system, constraint forces (springs/links) between the various rigid bodies and internal elastic forces within flexible members. The forces that are applied directly on the offshore wind turbine system include the hydrostatic, hydrodynamic and mooring forces on the floating platform, the aerodynamic forces acting on the blades and the tower and the gravitational forces acting on the entire wind turbine etc. It must be noted here that the gear box friction forces are neglected in this paper. Yaw springs and damper act as constraint forces between the tower and the nacelle. Elasticity of the tower, the blades and the low-speed shaft also contribute to the generalised active forces. Thus the total generalised active force can be given as

$$\begin{aligned} F_r = {} & F_r\big|_{HydroX} + F_r\big|_{AeroT} + F_r\big|_{AeroB1} + F_r\big|_{AeroB2} + F_r\big|_{AeroB3} + F_r\big|_{GravX} + F_r\big|_{GravT} \\ & + F_r\big|_{GravN} + F_r\big|_{GravH} + F_r\big|_{GravB1} + F_r\big|_{GravB2} + F_r\big|_{GravB3} + F_r\big|_{YawSprng} \\ & + F_r\big|_{YawDamp} + F_r\big|_{Gen} + F_r\big|_{Brake} + F_r\big|_{ElasticT} + F_r\big|_{ElasticB1} + F_r\big|_{ElasticB2} \\ & + F_r\big|_{ElasticB3} + F_r\big|_{DampT} + F_r\big|_{DampB1} + F_r\big|_{DampB2} + F_r\big|_{DampB3} + F_r\big|_{ElasticDrive} \\ & + F_r\big|_{DampDrive} \end{aligned} \tag{10}$$

Kane's equations of motion can be written in matrix form as

$$\mathbf{M}(\mathbf{q}, t)\ddot{\mathbf{q}} + \mathbf{f}(\dot{\mathbf{q}}, \mathbf{q}, t) = 0 \Rightarrow \mathbf{M}(\mathbf{q}, t)\ddot{\mathbf{q}} = -\mathbf{f}(\dot{\mathbf{q}}, \mathbf{q}, t) \tag{11}$$

The above equation can be readily solved by a computer using any numerical time integration scheme. This study recommends the use of Runga–Kutta 4th order method or the Adams-Bashforth-Moulton 4th order predictor–corrector method. The kinetic description of each individual component is provided in Appendix C.

2.5. Wave–Current Interaction Model

Airy wave theory is used to model the wave–current interaction considering the effect of an underlying current [37,38]. Two-dimensional flow is considered, i.e., waves travelling in a favourable and adverse direction to the underlying current. To describe the flow-field, a coordinate system is established with its origin placed on the mean water level (MWL) with the x-axis denoting the horizontal axis and the z-axis denoting the vertical axis pointing upwards as shown in Figure 3. In Figure 3, $\eta(x, t)$ denotes the time-varying water surface

elevation and $U(z)$ denotes the current velocity profile as a function of z without waves. The still water depth is denoted by h_w.
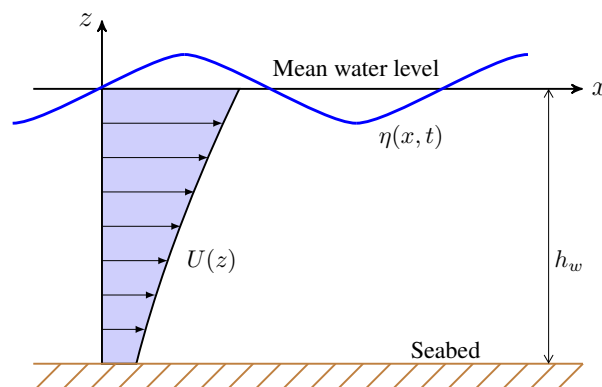

Figure 3. Coordinate system for wave–current interaction definition.

2.5.1. Regular Wave on Current

When the waves travelling on an underlying current has relatively small amplitudes, the velocity field can be expressed as the summation of the flow due to the current and surface wave as [39,40]

$$u_T(x,z,t) = U(z) + u(z)\cos(\kappa x - \omega t) \tag{12}$$

$$w_T(x,z,t) = w(z)\sin(\kappa x - \omega t) \tag{13}$$

where $U(z)$ is the current velocity as a function of z; ω and κ are the angular frequency and the wave number respectively. It must be noted that ω is the apparent frequency considering the effect of the underlying current [41]. In the above equations, $u_T(x,z,t)$ and $w_T(x,z,t)$ are the flow velocities in the horizontal and the vertical directions respectively, and $u(x,z,t)$ and $w(x,z,t)$ are the wave velocities using the first-order term [39] in the horizontal and the vertical directions respectively. Using the Airy wave theory, the free surface wave elevation η is obtained as

$$\eta(x,t) = A\cos(\kappa x - \omega t) \tag{14}$$

where $A =$ is the amplitude of the surface wave. For a given free surface function and a uniform or linear current profile, the flow velocity can be solved analytically $(\mathrm{d}^2 U(z)/\mathrm{d}z^2 = 0)$ (see [40] for details), as

$$u_T(x,z,t) = U(z) + A(\omega - \kappa U_0)\frac{\cosh[\kappa(z+h_w)]}{\sinh(\kappa h_w)}\cos(\kappa x - \omega t) \tag{15}$$

$$w_T(x,z,t) = A(\omega - \kappa U_0)\frac{\sinh[\kappa(z+h_w)]}{\sinh(\kappa h_w)}\sin(\kappa x - \omega t) \tag{16}$$

where $U_0 =$ the current velocity at $z = 0$. Futhermore, the corresponding dispersion relation is

$$(\omega - \kappa U_0)^2 = \left[g\kappa - (\omega - \kappa U_0)\frac{\mathrm{d}U}{\mathrm{d}z}\right]\tanh(\kappa h_w) \tag{17}$$

valid for uniform and linear shear currents. The flow field can be determined using Equations (15) and (16) after obtaining the wave numbers by solving Equation (17).

2.5.2. Irregular Waves on Current

To evaluate the effect of the underlying current on irregular waves, the Equations (15) and (16) are combined with a spectral model. The effect of the underlying current on the wave spectrum is modelled as [37]

$$S(\omega, U) = \frac{4S(\omega)}{\left(1 + \sqrt{1 + 4\omega U/g}\right)^2 \sqrt{1 + 4\omega U/g}} \tag{18}$$

where the expressions $S(\omega, U)$ and $S(\omega)$ denote the wave spectra with and without the current respectively. It can be noted that, as $\omega \to -g/4U$, the wave is unable to propagate against the current and the wave breaks. The above equation is valid only for $1 + 4\omega U/g > 0$ when waves are travelling on top of an adverse current. To handle the wave breaking case, refs. [42,43] defined an "equilibrium limit" for deep water as

$$S_{\mathrm{ER}}(\omega, U) = \frac{A^* g^2}{(\omega - kU)^5} \frac{1}{1 + 2U(\omega - \kappa U)/g} \tag{19}$$

where the equilibrium range is denoted by subscript ER and A^* is a constant between 0.008 and 0.015 [44]. During wave breaking, Equation (19) is used instead for a wave frequency when $S(\omega, U) > S_{\mathrm{ER}}(\omega, U)$.

Finally, the water surface elevation is expressed as

$$\eta(x, t) = \sum_{j=1}^{N} A_j \cos(k_j x - \omega_j t + \phi_j) \tag{20}$$

where ϕ_j is a uniformly distributed random phase angle between 0 to 2π and N denotes the number of wave components. The amplitude of the jth wave is given as $A_j = \sqrt{2S(\omega_j, U)\Delta\omega}$ with $\Delta\omega$ the frequency interval. The corresponding flow velocities are given as

$$u_T(x, z, t) = U(z) + \sum_{j=1}^{N} A_j(\omega_j - \kappa_j U) \frac{\cosh\left[\kappa_j(z + h_w)\right]}{\sinh(\kappa_j h_w)} \cos(\kappa_j x - \omega_j t + \phi_j) \tag{21}$$

$$w_T(x, z, t) = \sum_{j=1}^{N} A_j(\omega_j - \kappa_j U) \frac{\sinh\left[\kappa_j(z + h_w)\right]}{\sinh(\kappa_j h_w)} \sin(\kappa_j x - \omega_j t + \phi_j) \tag{22}$$

The accelerations can be obtained from the preceding equations, as

$$\dot{u}_T(x, z, t) = \sum_{j=1}^{N} A_j \omega_j(\omega_j - \kappa_j U) \frac{\cosh\left[\kappa_j(z + h_w)\right]}{\sinh(\kappa_j h_w)} \sin(\kappa_j x - \omega_j t + \phi_j) \tag{23}$$

$$\dot{w}_T(x, z, t) = -\sum_{j=1}^{N} A_j \omega_j(\omega_j - \kappa_j U) \frac{\sinh\left[\kappa_j(z + h_w)\right]}{\sinh(k_j h_w)} \cos(\kappa_j x - \omega_j t + \phi_j) \tag{24}$$

where the wave-number κ_j is obtained by solving Equation (17) for each wave component. Figure 4 presents an example of the Pierson–Moskowitz spectrum with and without an underlying linear current. The significant wave height is 3 m, the peak spectral period is 6 s and surface current velocity of the underlying uniform current profile is 0.609 m/s [45]. It can be observed that there is a reduction of the wave spectrum peak in the presence of an underlying current.
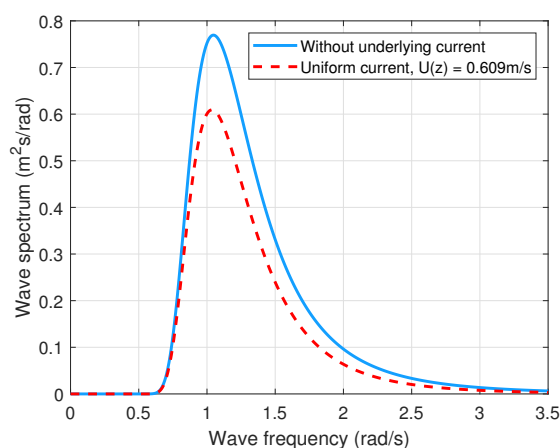
Figure 4. Pierson–Moskowitz spectrum with and without an underlying current.

2.6. Aerodynamic Loads

The popular Blade Element Momentum (BEM) theory is used in this paper to estimate the aerodynamic loads on the wind turbine. The TurbSim [46] package is used to create the 3D wind fields. TurbSim [46] generated wind fields account for spatial coherence of the turbulence along with vertical and horizontal wind shear. The package takes the characteristic wind speeds at a reference height, turbulence intensity level, and wind power-law coefficients for wind shear as some of the primary inputs. The BEM program used in this paper interpolates the wind speeds at the blade nodes from the TurbSim wind fields. It estimates aerodynamic loads using the blades' quasi-static aerodynamic properties (i.e., lift and drag). The BEM theory is widely available in the literature [47–49] and is not repeated here.

A new solution approach proposed by Ning [50] was used here to solve the BEM equations. In this approach, a 1D root finding method (`fzero` in MATLAB) is to find the unknown inflow angle instead of solving the three-dimensional problem of finding the tangential and the axial induction factors. Different equations are used in the momentum, empirical, and propeller brake region to form the solution in this approach. Furthermore, the empirical region is modified using Glauert's correction with Buhl's modification. As described by [50], using different equations for the different regions enables us to circumvent the traditional two-point iterative procedure of solving the BEM equations. To account for the vortices generated by the blade tips and the hub, Prandtl's hub, and tip loss correction factors are also included in the program. The Pitt and Peters correction for skewed inflow has also been included in the program. The solution of the BEM equations at a radial distance *r* gives the lift and drag forces on the blades a radial distance *r* from the root of the blade. The out-of-plane force (thrust) and in-plane force (torque) on the blades is then estimated from the lift and drag forces. These forces are then integrated along the length of the blades to obtain the total forces on the blades. For details on the procedure, please refer to [51].

2.7. Hydrodynamic Loads

The hydrodynamic loads on the cylindrical spar of the wind turbine is estimated using Morison's equation. Morison's equations together with strip theory is used to estimate the linear wave inertia forces and the non-linear viscous drag forces. The total wave loads on the platform is estimated by integrating the elemental forces along the length/depth of the platform. The hydrodynamic forces on a strip dz of the platform in surge and sway directions respectively are given as

$$dF_i^P(z,t) = \underbrace{-C_A\rho\left(\frac{\pi D(z)^2}{4}\right)\ddot{q}_i(z,t)dz}_{\text{added mass}} + \underbrace{C_M\rho\left(\frac{\pi D(z)^2}{4}\right)a_i^f(z,t)dz}_{\text{fluid inertial force}}$$
$$+ \underbrace{\frac{1}{2}C_D\rho D(z)\left(v_i^f(z,t) - v_i^p(z,t)\right)|v_i^f(z,t) - v_i^p(z,t)|dz}_{\text{viscous drag force}} \quad \text{for } i = Sg, Sw \quad (25)$$

where dF_i^P is the elemental force on the platform along the ith degree of freedom. The rolling and pitching moments on the platform can be obtained as

$$dM_i^P(z,t) = \begin{cases} -dF_{Sg}^P(z,t)z & i = P \\ dF_{Sw}^P(z,t)z & i = R \end{cases} \quad (26)$$

where dM_i^P is the moment per unit length on the platform for the ith degree of freedom. The total forces and moments on the platform are obtained by integrating the distributed forces and moments along the length/depth of the platform. For the symmetrical spar, the heave force and the yaw moment are assumed to be zero. Morison's equations assume that viscous drag forces dominate the total drag forces on the platform and the radiation damping is negligible. This assumption is valid when the cylinder diameter is small compared to the wavelength and the platform's small motion. It must be noted that Equation (25) does not include the added mass associated with the platform heave degree of freedom. Hence, added mass coefficient as per [18] is included in this paper for the heave degree of freedom.

2.8. Mooring Dynamics Model

OpenMOOR [52] is used to estimate the mooring force on the platform in this paper. OpenMOOR is an open-source mooring system simulation program developed by L Chen et al. [52] that can be used to estimate the mooring forces at a reference point on a platform. The program is developed based on the model of submerged cables [53–55], as shown in Figure 5. The cables are modelled as Euler beams, including the effects of its bending and torsional stiffness. The hydrodynamic forces are included using the modified Morison's equations. For the part of the cable grounded on the seabed, the seabed is modelled as a flat visco-elastic mattress. The seabed stiffness was obtained from the FAST [25] case files. The cable fairlead forces and consequently the FOWT motion are not sensitive to the value of the seabed stiffness as reported in the literature and verified here using a parametric analysis. However, it must be noted that the seabed stiffness is important in case of fatigue analysis of the cable near the touchdown point. When using OpenMOOR to solve for the mooring forces, the fairlead motion is first computed using the multi-body dynamics (in this case, the wind turbine). Then the two-point boundary problem for all three cables is solved parallelly using the generalised-α method for both spatial and temporal discretization [55]. A Newton-like method with dynamic relaxation is used to solve the resulting non-linear algebraic equation. OpenMOOR is also capable of including steady ocean currents of arbitrary profiles. In this paper, the effect of waves on the mooring cable is ignored as the fairleads of the turbine are deep below the mean water level (MWL), where currents are predominant. In this work, OpenMOOR is separately compiled into a dynamic linking library and imported/coupled with the multi-body dynamic model of the FOWT in MATLAB®.
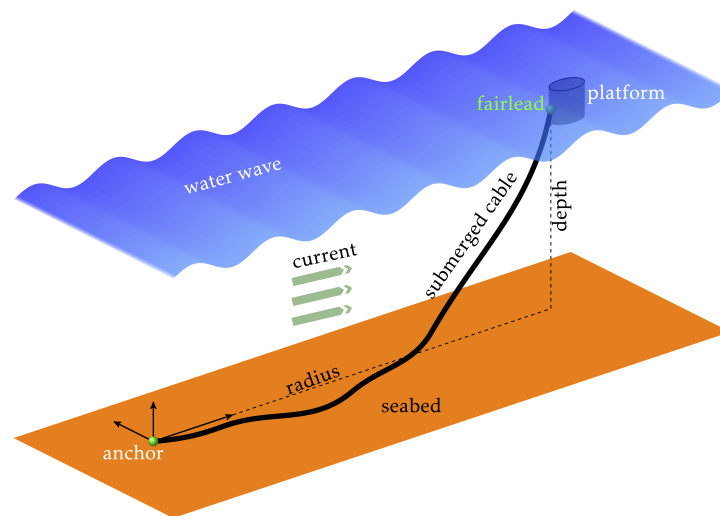
Figure 5. Submerged cable subjected to wave and current [30].

The multi-body code of the FOWT is coupled with OpenMoor. The displacements and velocities of the platform reference points are sent to OpenMoor, and the estimated mooring loads are applied on the platform. This soft-coupling creates a one-time step time lag between the platform/wind turbine state and OpenMoor loads. However, the error becomes insignificant with a sufficiently small time step, and this requirement can be waived. A similar practice can be found in state-of-the-art simulation tools like FAST [25].

2.9. Structural Control—Passive TMDI Installed on Tower-Top

In this section a passive Tuned Mass Damper Inerter (TMDI) is installed inside the top of the tower to mitigate vibrations of the wind turbine tower. The damper is installed in the tower as shown in Figure 6.
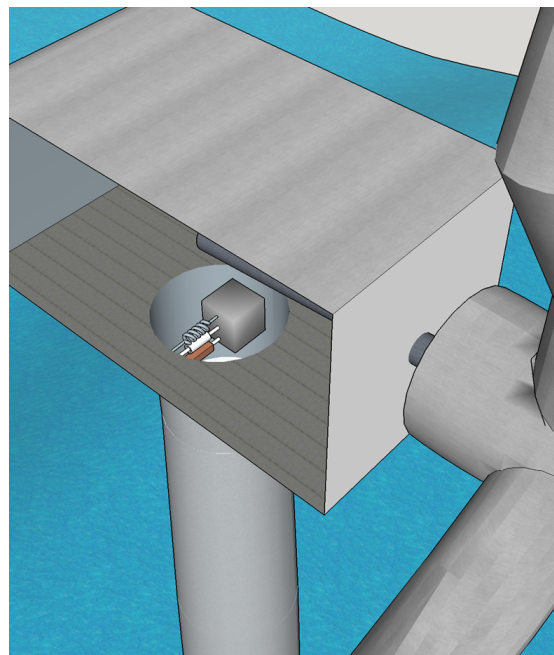

Figure 6. TMDI installed inside tower [31].

The TMDI is a relatively new concept in which an 'inerter' device (mechanical flywheel-based device in this case) is attached in parallel to the linear spring and the linear damper to the mass of a classical tuned mass damper (TMD). The inerter transforms the linear translation of the tuned mass into a rotation of the flywheels to provide a mass

amplification effect on the classical TMD. The mass amplification effect increases the device's vibration control capabilities, enabling one to achieve enhanced vibration control using a relatively lighter damper. Several recent studies have investigated the use of TMDIs for vibration control of FOWTs [31,56,57]. This section will demonstrate the procedure of installing a TMDI device inside a FOWT using Kane's method and will emphasise the relative ease of the procedure compared to traditional energy formulation-based methods.

Installing a TMDI in the tower is straightforward because the position of the essential points on the wind turbine is not dependent on the position of the TMDI mass. The position of the TMDI mass is denoted by the new generalised coordinate q_{TMDI} which is also denoted by the number 23. Therefore, the position vectors, velocity vectors, etc. derived previously do not change. Only the position vector of the TMDI mass needs to be derived, followed by its partial linear velocities and acceleration. The kinematic and kinetic description of the TMDI placed on top of the tower is provided in Appendix D. The resulting system matrices of the TMDI superimposed on the overall system matrices result in the coupled system matrices of the FOWT-TMDI system.

2.9.1. TMDI Parameter Optimization Using a Simplified Model

The floating offshore wind turbine system coupled with a TMDI system has a complicated set of non-linear equations of motion that cannot optimise the TMDI properties in closed form. Therefore, to derive the optimal properties of the TMDI, a couple of simplifications have been made

- A 2-DOF system with the TMDI represents the wind turbine placed on top of the tower as shown in Figure 7.
- The wind turbine is subjected to white noise.
- The mass of the blades, the hub, and the nacelle are lumped on top of the tower and its base is fixed.
- The inerter is hooked between the mass of the damper and the tower at an arbitrary height H_I from the base of the tower.
- The primary structure, in this case, the wind turbine tower, does not offer any damping.

Under the above assumptions, the governing equations of motion normalised by the mass of the primary structure m_0 is given as

$$
\begin{bmatrix} 1 + \mu + \beta(1-\phi)^2 & \mu + \beta(1-\phi) \\ \mu + \beta(1-\phi) & \mu + \beta \end{bmatrix} \begin{pmatrix} \ddot{q}_t \\ \ddot{q}_d \end{pmatrix} + \begin{bmatrix} 0 & 0 \\ 0 & 2\mu\omega_t\zeta_d\omega_r \end{bmatrix} \begin{pmatrix} \dot{q}_t \\ \dot{q}_d \end{pmatrix}
$$
$$
+ \begin{bmatrix} \omega_t^2 & 0 \\ 0 & \mu\omega_t^2\omega_r^2 \end{bmatrix} \begin{pmatrix} q_t \\ q_d \end{pmatrix} = \begin{pmatrix} \frac{F}{m_0} \\ 0 \end{pmatrix} \tag{27}
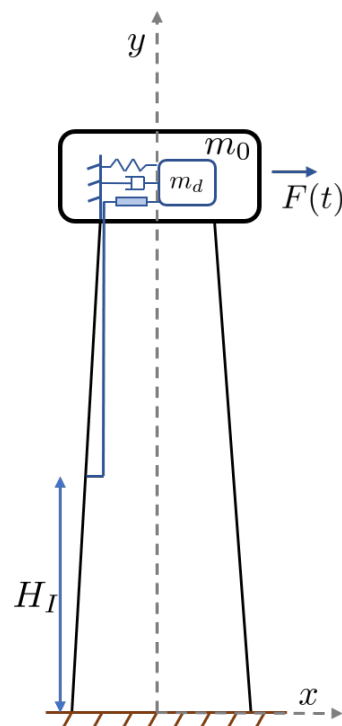$$

Figure 7. Schematic diagram of a tower with a TMDI placed on the top.

q_t and q_d denotes the tower and the damper degrees of freedom respectively. μ is the mass ratio and β is the inerter ratio defined as

$$\mu = \frac{m_d}{m_0} \qquad \beta = \frac{b}{m_0} \tag{28}$$

where m_d is the damper mass and b is the inertance [58]. b has the units of mass and details can be found in [58,59]. The tuning ratio and damping ratio of the damper are defined as

$$\omega_r = \frac{\omega_d}{\omega_t} \qquad \zeta_d = \frac{c_d}{2m_d\omega_d} \tag{29}$$

where ω_t and ω_d are the natural frequency of the tower and the damper respectively, and c_d is the damping coefficient of the TMDI. The normalised (normalised to 1) displacement of the tower at a height H_I from its base can be obtained directly from the primary mode shape as

$$\phi = \phi_t(H_I) \qquad \text{where } 0 \leq \phi \leq 1 \tag{30}$$

where ϕ_t is the primary mode shape of the tower. F is the white noise excitation force of constant intensity. For such a system the optimum tuning parameters were obtained by [31] as

$$\omega_r = \sqrt{\frac{-B + \sqrt{B^2 - AC}}{2A}} \tag{31}$$

where

$$A = 3\mu^2(\mu^2 + 2\mu\phi^2\beta - 4\mu\phi\beta + 2\mu\beta + 2\mu + \phi^4\beta^2 - 4\phi^3\beta^2 + 6\phi^2\beta^2 + 2\phi^2\beta - 4\phi\beta^2$$
$$- 4\phi\beta + \beta^2 + 2\beta + 1)$$
$$B = \mu(4\mu^2\zeta_d^2 - \mu^2 + 4\mu\phi^2\zeta_d^2\beta - 2\mu\phi^2\beta - 8\mu\phi\zeta_d^2\beta + 2\mu\phi\beta + 4\mu\zeta_d^2\beta + 4\mu\zeta_d^2 - 2\mu\beta$$
$$- 2\mu - \phi^2\beta^2 + 2\phi\beta^2$$
$$- \beta^2 - 2\beta)$$
$$C = -(\mu^2 + 2\mu\beta + \beta^2)$$

and the optimal damping ratio

$$\zeta_d = \frac{1}{2\mu\omega_r}\sqrt{\frac{D}{E}} \tag{32}$$

where

$$D = \mu^4\omega^4 + 2\mu^3\phi^2\beta\omega_r^4 - 4\mu^3\phi\beta\omega_r^4 + 2\mu^3\beta\omega_r^4 + 2\mu^3\omega_r^4 - \mu^3\omega_r^2 + \mu^2\phi^4\beta^2\omega_r^4$$
$$- 4\mu^2\phi^3\beta^2\omega_r^4 + 6\mu^2\phi^2\beta^2\omega_r^4 + 2\mu^2\phi^2\beta\omega_r^4 - 2\mu^2\phi^2\beta\omega_r^2 - 4\mu^2\phi\beta^2\omega_r^4$$
$$- 4\mu^2\phi\beta\omega_r^4 + 2\mu^2\phi\beta\omega_r^2 + \mu^2\beta^2\omega_r^4 + 2\mu^2\beta\omega_r^4 - 2\mu^2\beta\omega_r^2 + \mu^2\omega_r^4 - 2\mu^2\omega_r^2 + \mu^2$$
$$- \mu\phi^2\beta^2\omega_r^2 + 2\mu\phi\beta^2\omega_r^2 - \mu\beta^2\omega_r^2 - 2\mu\beta\omega_r^2 + 2\mu\beta + \beta^2$$
$$E = \mu + \phi^2\beta - 2\phi\beta + \beta + 1$$

Note that Equations (31) and (32) reduce to the optimal tuning parameters for classical TMD(s) when $b = \beta = 0$ and the primary structure is excited by white noise. In addition, note that Equations (31) and (32) are coupled. Hence, an iterative procedure must to used with a sufficiently small tolerance to find the optimal parameter. It is found that a simple iterative scheme is capable for finding the solution with sufficient speed and accuracy.

3. Results and Discussion

The previous section detailed the method of deriving the equations of motion of a FOWT and the associated dynamic (aerodynamic and hydrodynamic) loads. To demonstrate the accuracy of the developed dynamic model, the developed model is compared and validated against state-of-the-art wind turbine simulator FAST [25]. The results are provided in the following sub-section. Next, the performance of a optimally tuned TMDI is investigated in the following sub-section.

3.1. Benchmarking against FAST v8

All numerical codes used to model the FOWT are developed in MATLAB®. In this section, the floating offshore wind turbine model developed in this study is validated against the state-of-the-art wind turbine simulator FAST [25] using code-to-code comparison. The spar type FOWT multi-body dynamic model developed theoretically is instantiated using the details provided from the NREL 5 MW baseline offshore wind turbine [60]. The basic properties of the floating wind turbine are provided in Table 1, for more details on the wind turbine, please refer to [60]. The offshore wind turbine is simulated under a steady (rated) wind speed of 11.4 m/s in still water for verification purposes. The aerodynamic loads are calculated using the Blade Element Momentum Theory (BEM), as described previously. The verification results for the primary structural responses are shown in Figure 8. The other responses of the offshore wind turbine are provided in Figure A1 in Appendix F. A comparison of the time histories after the initial transient phase (50 s) is presented in terms of the mean, standard deviation, and max/min values in Table 2. The numerical results compare satisfactorily with FAST [25] which numerically verifies the developed multi-body model using Kane's method.

The responses of the floating offshore wind turbine tower, blades, nacelle, and low-speed shaft match very well with the ones obtained from FAST [25] as shown in Figure 8. However, minor dissimilarities are observed in the platform motion in Figure A1. A phase shift can be observed in the floating platform response time histories. While FAST [25] includes radiation forces from the linear potential flow theory together with viscous drag forces from Morison's equation, the model derived here only includes the viscous drag forces from Morison's equation. The difference in the resulting hydrodynamic damping forces manifests a phase shift in the response time histories. It is also noteworthy that the degrees of freedom that are subjected to lower levels of hydrodynamic damping like the platform surge, the platform heaves or reaches steady state quickly like platform pitch and the platform yaw is less affected by this phase shift. The degrees of freedom most affected by this phase shift are the platform sway and roll degrees of freedom. However, it can be observed that the mean and the frequency content of all of the responses match very well with FAST [25] which is most important from a dynamic analysis point of view.

Table 1. Basic properties of the NREL 5 MW baseline offshore wind turbine.

Baseline turbine properties	
Rating	5 MW
Rotor orientation, no of blades	Upwind, 3 blades
Rotor diameter, hub diameter	126 m, 3 m
Hub height	90 m
Cut-in, rated, cut-out wind speeds	3 m/s, 11.4 m/s, 25 m/s
Cut-in, rated rotor speeds	6.9 RPM, 12.1 RPM
Rated tip speed	80 m/s
Control	Variable speed, collective pitch
Drivetrain	3-stage gearbox
Overhang, shaft tilt, precone	5 m, 5°, 2.5°
Tower properties	
Elevation of tower base from SWL	10 m
Elevation of tower top from SWL	87.6 m
Floating platform properties	
Depth of platform base below SWL	120 m
Elevation of platform top above SWL	10 m
Depth to top of taper below SWL	4 m
Depth to bottom of taper below SWL	12 m
Platform diameter above taper	6.5 m
Platform diameter below taper	9.4 m

Table 2. Comparison of response statistic between FAST and the derived model (DM).

| Response	Mean		Min		Max		Std.	
	FAST	DM	FAST	DM	FAST	DM	FAST	DM
Blade OOP displacement (m)	5.283	5.296	4.396	4.366	5.971	6.037	0.448	0.477
Blade IP displacement (m)	−0.559	−0.565	−1.085	−1.090	−0.038	−0.046	0.354	0.353
Tower-top FA displacement (m)	0.460	0.458	0.436	0.431	0.481	0.478	0.011	0.011
Tower-top SS displacement (m)	−0.051	−0.051	−0.058	−0.062	−0.040	−0.040	0.003	0.003
Nacelle yaw angle (°)	2.2E-3	2.2E-3	7.1E-4	6.1E-4	3.8E-3	3.8E-3	1.0E-3	1.0E-3
Rotor speed (RPM)	11.910	11.899	11.840	11.834	11.970	11.959	0.035	0.035
Platform surge (m)	25.075	24.872	20.380	20.009	30.830	30.837	3.430	3.564
Platform sway (m)	−0.319	−0.309	−0.359	−0.372	−0.261	−0.253	0.026	0.027
Platform heave (m)	−0.589	−0.611	−0.961	−0.968	−0.377	−0.417	0.133	0.131
Platform roll (rad)	4.4E-3	4.4E-3	3.7E-3	3.4E-3	5.1E-3	5.3E-3	2.95E-4	4.45E-4
Platform pitch (rad)	0.085	0.086	0.079	0.079	0.090	0.090	3.1E-3	2.9E-3
Platform yaw (rad)	3.9E-3	3.9E-3	3.5E-3	3.6E-3	4.4E-3	4.5E-3	2.1E-4	2.1E-4
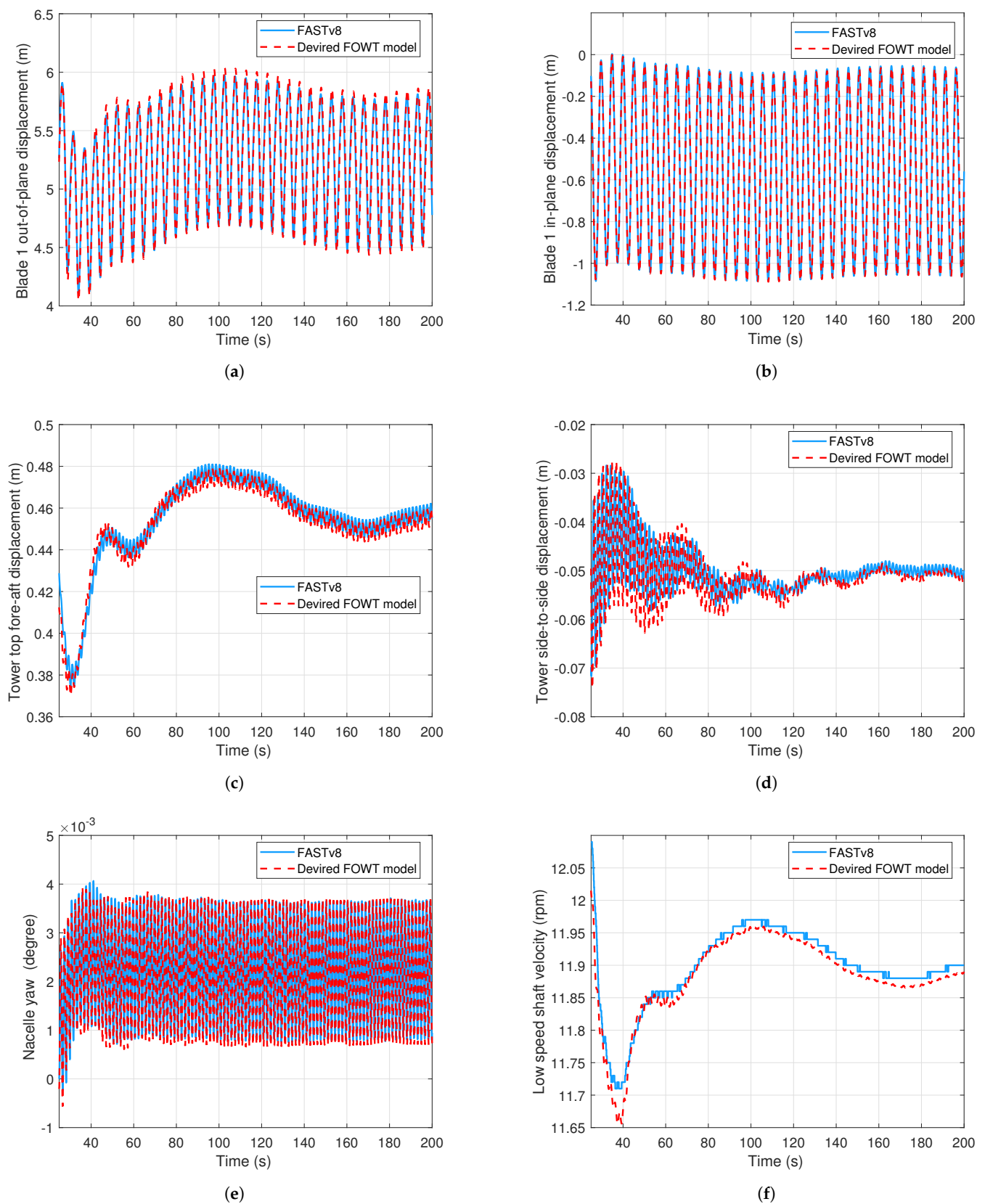
Figure 8. Model verification: motion of the floating offshore wind turbine. (**a**) Blade 1 out-of-plane displacement; (**b**) Blade 1 in-plane displacement; (**c**) Tower top fore-aft displacement; (**d**) Tower to side-to-side displacement; (**e**) Nacelle yaw rotation; (**f**) Low speed shaft speed.

3.2. Performance of the Passive TMDI

The TMDI is coupled to the baseline offshore wind turbine [60] used earlier in this study. The TMDI is optimised according to Section 2.9.1. The damper's performance has been investigated over an extensive range of wind-wave loading environments by the authors in [31]. In this paper, only one case of met-ocean condition is presented for illustrative purposes. The chosen met-ocean condition has a hub-height mean wind speed of 20 m/s, a significant wave height of 6 m, and a peak spectral period of 8 s. The TMDI is installed in the nacelle, has 1% of the tower mass (excluding the RNA), and is tuned to the tower's natural frequency. The tower side-to-side motion with and without the TMDI is shown in Figures 9 and 10. Futhermore, the tower fore-aft motion with and without the TMDI is shown in Figures 11 and 12. Excellent damping of the tower side-to-side vibrations is observed using a damper having a mass of just 1% of the tower mass. On the other hand, the vibration reduction for the fore-aft motion of the tower is modest as the fore-aft modes experience considerable aerodynamic damping. The figures also include a case where the inerter ratio β is zero, reducing the TMDI to a classical TMD. It can be observed that, expectantly, the performance of the classical TMD is considerably worse than the TMDI.

Another critical aspect of the TMDI is the drastic reduction of tuned mass stroke. The comparison of the damper stroke between a classical TMD and a TMDI is shown in Figures 13 and 14. The authors also showed in [31] that increasing the mass ratio of the damper to improve vibration reduction is not a good idea for floating offshore wind turbines. Increasing the mass lumped on top of the tower will destabilise the floating platform. For more details on vibration control of floating offshore wind turbine towers using TMDI(s), refer to [31].
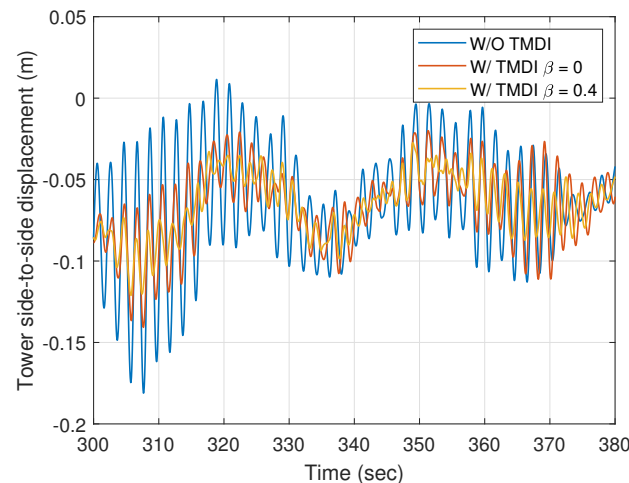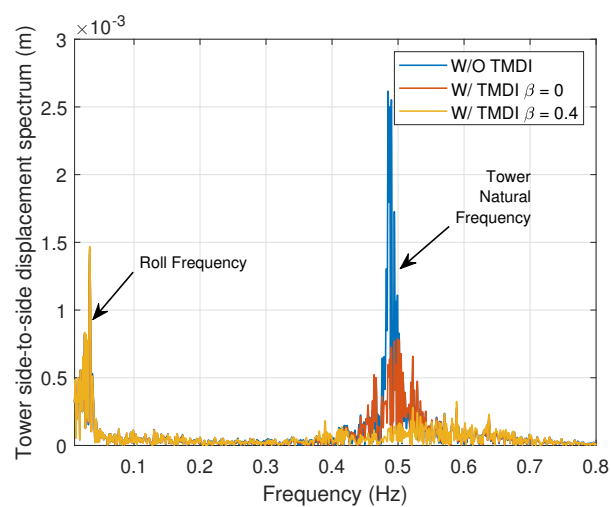

Figure 9. Tower side-to-side displacement.
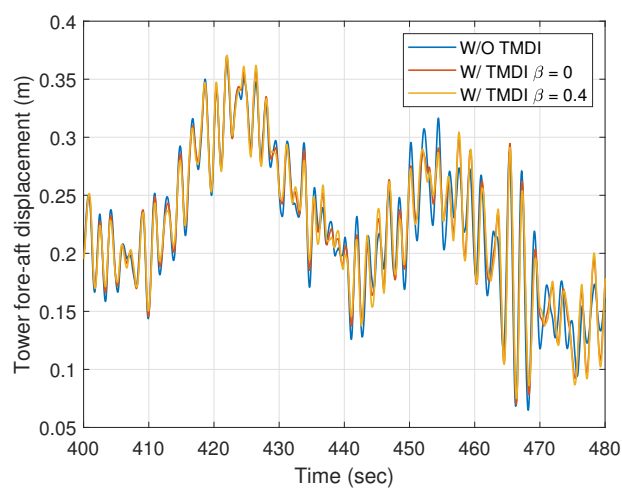
Figure 10. Tower side-to-side displacement spectrum.

Figure 11. Tower fore-aft displacement.
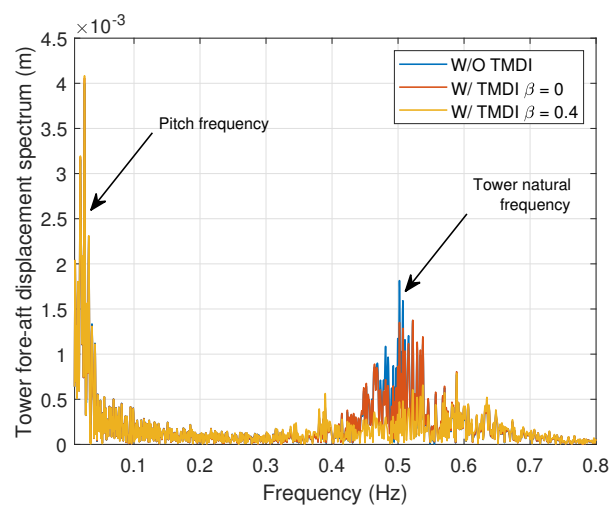

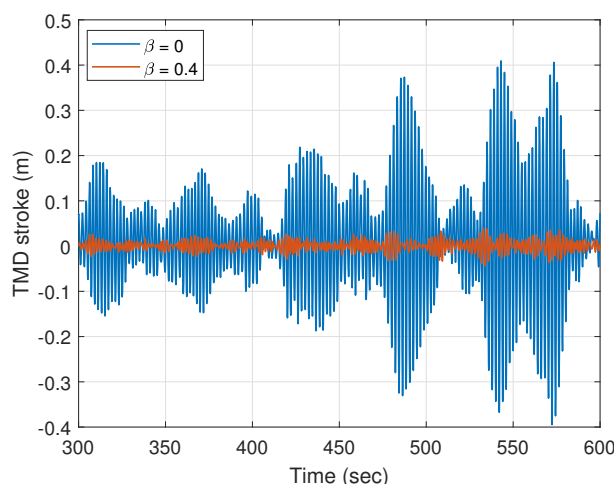**Figure 12.** Tower fore-aft displacement spectrum.

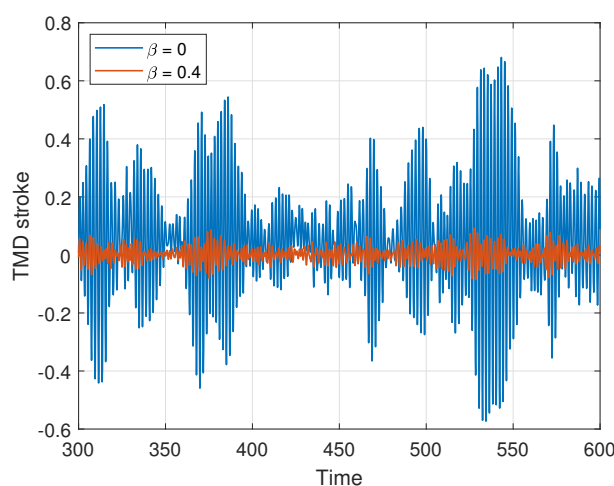**Figure 13.** Tower side-to-side damper stroke.

Figure 14. Tower fore-aft damper stroke.

4. Conclusions

This paper demonstrated the use of Kane's method for deriving equations of motion for spar-type floating offshore wind turbines, the steps of which apply to any multi-body system. The flexible multi-body wind turbine was modelled as a system comprising flexible and rigid members. Each component was modelled in its local coordinate system and transformed back to the inertial frame of reference using suitable transformation relationships. The derived model was benchmarked against the industry standard FAST [25]. Kane's method was further used for the installation of an external damper. The excellent performance of the recently conceptualised TMDI in vibration control of floating offshore wind turbine towers was also presented.

It has been shown in this paper that Kane's method vastly reduces the labor needed to derive equations of motion of a complicated multi-degree of freedom system. The resulting equations of motion are obtained as ODEs (rearrangement of terms not required), and the required vector multiplications can be performed on a computer. Therefore, the equations of motion are formed directly on a computer without human intervention, which is particularly desirable when working with many variables. The paper also demonstrates Kane's method's ease in installing an external device on the wind turbine.

As described in this paper, a large number of vector multiplications are performed on a computer to evaluate kinematics and kinetics of the system. A limitation of this method

is the increasing computational time with increasing complexity of the system. However, with the rapid increase in computational power, it is unlikely to hinder performance.

Lastly, it is essential to mention that Kane's method presented in this paper is general and applicable to any offshore/onshore wind turbine. Therefore, the steps are general to any dynamic system. This project envisages the use of this powerful modeling technique in extending the capabilities of the current wind turbine models. Some examples are as follows, installation of auxiliary devices [31], modification of current structural arrangements and components [61,62]. Investigation of improved foundation techniques and modeling future wind turbines. [63] etc. The developed knowledge will be used for modeling and dynamic analysis of the future larges-scale wind turbines.

Abbreviations

The following abbreviations are used in this manuscript:

$LSS - S$	Low speed shaft-skew angle (rad)
$LSS - T$	Low speed shaft-tilt angle (rad)
$TwrHt$	Height of the wind turbine tower (m)
$PreCone$	Blade cone angles (rad)
$BlPit$	Blade pitch angles (rad)
$PtfmCMzt$	Vertical distance from the MSL to the platform CM (m)
$PtfmRefzt$	Vertical distance from the MSL to the platform reference point (m)
$NacCMxn$	Downwind distance from the tower-top to the nacelle CM (m)
$NacCMzn$	Vertical distance from the tower-top to the nacelle CM (m)
$NacCMyn$	Lateral distance from the tower-top to the nacelle CM (m)
$Overhang$	Distance from yaw axis to rotor apex [3 blades] (m)
$Twr2Shft$	Vertical distance from the tower-top to the rotor shaft (m)
$Yaw2Shft$	Lateral distance from the tower center line to the rotor shaft (m)
$HubCM$	Distance from rotor apex to hub mass [positive downwind] (m)
$HubRad$	Hub Radius
$GenDir$	Generator direction
GBR	Gear Box ratio
$GenIner$	Generator inertia about HSS (kg m^2)
$TFA1$	First fore-aft tower bending-mode
$TFA2$	Second fore-aft tower bending-mode
$TSS1$	First side-to-side tower bending-mode
$TSS2$	Second side-to-side tower bending-mode
$GeAz$	Generator azimuth angle
$DrTr$	Drive-train torsion
$BiF1$	First flapwise bending-mode of ith blade
$BiF2$	Second flapwise bending-mode of ith blade
$BiE1$	First edgewise bending-mode of ith blade
Sg	Platform surge

Sw	Platform sway
Hv	Platform heave
R	Platform roll
P	Platform pitch
Y	Platform yaw
FA	Fore-aft
SS	Side-to-side
OOP	Out-of-plane
IP	In-plane
$PtfmRIner$	Platform inertia for roll tilt rotation about the platform CM (kg m^2)
$PtfmYIner$	Platform inertia for yaw rotation about the platform CM (kg m^2)
$PtfmPIner$	Platform inertia for pitch tilt rotation about the platform CM (kg m^2)
$YBMass$	Yaw bearing mass (kg)
$YawSpring$	Nacelle-yaw spring constant (N-m/rad)
$YawDamp$	Nacelle-yaw damping constant (N-m/(rad/s))
$NacYIner$	Nacelle inertia about yaw axis (kg m^2)
$HubIner$	Hub inertia about rotor axis (kg m^2)
$BlLn$	Flexural length of the blade
HSS	High speed shaft
LSS	Low speed shaft
$DTTorSpr$	Drive-train torsional spring (N-m/rad)
$DTTorDmp$	Drive-train torsional damper (N-m/(rad/s))
TMD	Tuned mass damper
$TMDI$	Tuned mass damper inerter

Appendix A. Symbols

The following symbols are used in this manuscript:

q_{Sg}	Platform surge DOF
q_{Sw}	Platform sway DOF
q_{Hv}	Platform heave DOF
q_R	Platform roll DOF
q_P	Platform pitch DOF
q_Y	Platform yaw DOF
q_{TFA1}	First tower fore-aft bending mode DOF
q_{TFA2}	Second tower fore-aft bending mode DOF
q_{TSS1}	First tower side-to-side bending mode DOF
q_{TSS2}	Second tower side-to-side bending mode DOF
q_{yaw}	Nacelle yaw DOF
q_{GeAz}	Generator azimuth angle DOF
q_{DrTr}	Drive-train torsional flexibility DOF
q_{BiF1}	First flapwise bending mode for ith blade DOF
q_{BiF2}	Second flapwise bending mode for ith blade DOF
q_{BiE1}	First edgewise bending mode for ith blade DOF
q_{TMD}	Tuned mass damper DOF
$\theta_{SS}(h)$	Tower side-to-side rotation (rad)
$\theta_{FA}(h)$	Tower fore-aft rotation (rad)
$\theta_s^{Bi}(r)$	Structural pre-twist of blades (rad)
$\theta_x^{Bi}(r)$	Blade out-of-plane rotation (rad)
$\theta_y^{Bi}(r)$	Blade in-plane rotation (rad)
$\mu^T(h)$	Tower mass per unit length (kg/m)
m^N	Nacelle mass (kg)
m^H	Hub mass (kg)
μ^B	Blade per unit length of ith blade (kg/m)

ϕ_1^{TFA}	First fore-aft tower mode shape
ϕ_2^{TFA}	Second fore-aft tower mode shape
ϕ_1^{TSS}	First side-to-side tower mode shape
ϕ_2^{TSS}	Second side-to-side tower mode shape
ϕ_1^{BiF}	First flapwise blade *i* mode shape
ϕ_2^{BiF}	Second flapwise blade *i* mode shape
ϕ_1^{BiE}	First edgewise blade *i* mode shape
C_A	Normalised hydrodynamic-added-mass coefficient in Morison's equation
C_M	Normalised mass (inertia) coefficient in Morison's equation
C_D	Normalised viscous-drag coefficient in Morison's equation
h_{TMDI}	Vertical distance of TMDI centre of mass from tower top
b	Inertance constant of the TMDI
m_{TMDI}	Mass of the TMDI
k_{TMDI}	Linear stiffness of the TMDI
ζ_{TMDI}	Linear damping ratio of the TMDI
f_{TMDI}	Natural frequency of the TMDI

Appendix B. Kinematics

This section describes the coordinates systems: the kinematic of the floating offshore wind turbine. The various quantities defined in this section facilitate the development of the equations of motion of the complete non-linear system.

Appendix B.1. Coordinate Systems

A set of inertial coordinate system $\hat{z}$ is fixed to the earth. Then, a set of coordinate system is attached to the base of the tower. The transformation relation can be obtained as

$$\begin{pmatrix} \hat{a}_1 \\ \hat{a}_2 \\ \hat{a}_3 \end{pmatrix} = T_O(\theta_1 = q_R, \theta_2 = q_Y, \theta_3 = -q_P) \begin{pmatrix} \hat{z}_1 \\ \hat{z}_2 \\ \hat{z}_3 \end{pmatrix} \tag{A1}$$

where q_R, q_Y and q_P are the roll, yaw and pitch degrees of freedom of the platform respectively. The tower element fixed coordinate system along the height of the tower can be obtained from the elastic deformation of the tower as

$$\begin{pmatrix} \hat{t}_1(h) \\ \hat{t}_2(h) \\ \hat{t}_3(h) \end{pmatrix} = T_O(\theta_{SS}(h), 0, -\theta_{FA}(h)) \begin{pmatrix} \hat{a}_1 \\ \hat{a}_2 \\ \hat{a}_3 \end{pmatrix} \tag{A2}$$

where $\theta_{SS}(h)$ and $\theta_{FA}(h)$ are the tower rotations in the side-to-side and fore-aft directions respectively at various sections along the height of the tower. The rotations are due to elastic deformation of the tower and can be obtained from the spacial derivatives of the mode shapes. Here, it must be noted the torsion of the tower is neglected because the yaw bearing is used to release the torsional moment. Next, the tower top/base plate coordinate system is defined as

$$\begin{pmatrix} \hat{b}_1 \\ \hat{b}_2 \\ \hat{b}_3 \end{pmatrix} = T_O(\theta_{SS}(Ht), 0, -\theta_{FA}(Ht)) \begin{pmatrix} \hat{a}_1 \\ \hat{a}_2 \\ \hat{a}_3 \end{pmatrix} \tag{A3}$$

where Ht is the flexural height of the tower. For reference frame where the orientation can be described by a simple rotation, Euler rotation matrix is used to transform the set of coordinates into the new frame. $R_x(\theta), R_y(\theta), R_z(\theta)$ represent anti-clockwise rotation

by an angle θ about x, y and z respectively. Hence, the nacelle yaw coordinate system is rotated about $\hat{b}_2$ axis by the yaw angle (q_{yaw}) of the nacelle and can be defined as

$$\begin{pmatrix} \hat{d}_1 \\ \hat{d}_2 \\ \hat{d}_3 \end{pmatrix} = R_{\hat{b}_2}(q_{yaw}) \begin{pmatrix} \hat{b}_1 \\ \hat{b}_2 \\ \hat{b}_3 \end{pmatrix} \tag{A4}$$

The shaft is often tilted and sometimes skewed with respect to the tower top. The coordinate system attached to the shaft can be given as

$$\begin{pmatrix} \hat{c}_1 \\ \hat{c}_2 \\ \hat{c}_3 \end{pmatrix} = R_{\hat{d}_2}(LSS - S) R_{\hat{d}_3}(LSS - T) \begin{pmatrix} \hat{d}_1 \\ \hat{d}_2 \\ \hat{d}_3 \end{pmatrix} \tag{A5}$$

where $LSS - S$ and $LSS - T$ denotes shaft-skew and shaft-tilt angles respectively. The azimuth coordinate system is also attached to the low speed shaft but rotates with the rotor and is defined next as

$$\begin{pmatrix} \hat{e}_1 \\ \hat{e}_2 \\ \hat{e}_3 \end{pmatrix} = R_{\hat{c}_1}(q_{DrTr} + q_{GeAz}) \begin{pmatrix} \hat{c}_1 \\ \hat{c}_2 \\ \hat{c}_3 \end{pmatrix} \tag{A6}$$

The rotation angle is summation of the generator azimuth angle (q_{GeAz}) and the torsional rotation of the drive train (q_{DrTr}). The coordinate system for blade 1 ($\hat{g}_1^{B1}, \hat{g}_2^{B1}, \hat{g}_3^{B1}$) is obtained as shown in Figure 2. As convention to three bladed wind turbines, the blades are $120°$ degrees apart. Next, the blade coned coordinate system is defined as

$$\begin{pmatrix} \hat{i}_1^{B1} \\ \hat{i}_2^{B1} \\ \hat{i}_3^{B1} \end{pmatrix} = R_{\hat{g}_2^{B1}}(PreCone(1)) \begin{pmatrix} \hat{g}_1^{B1} \\ \hat{g}_2^{B1} \\ \hat{g}_3^{B1} \end{pmatrix} \tag{A7}$$

The coned coordinate system for blade 2 and 3 can be defined similarly. The pitched coordinate system is defined as

$$\begin{pmatrix} \hat{j}_1^{B1} \\ \hat{j}_2^{B1} \\ \hat{j}_3^{B1} \end{pmatrix} = R_{\hat{i}_3^{B1}}(-BlPit(1)) \begin{pmatrix} \hat{i}_1^{B1} \\ \hat{i}_2^{B1} \\ \hat{i}_3^{B1} \end{pmatrix} \tag{A8}$$

where $BlPit$ are blade pitch angles. Again, the pitched coordinate system for blades 2 and 3 can be defined similarly. The blade coordinate system aligned to the local structural axes is defined as

$$\begin{pmatrix} \hat{l}_1^{B1}(r) \\ \hat{l}_2^{B1}(r) \\ \hat{l}_3^{B1}(r) \end{pmatrix} = R_{\hat{j}_3^{B1}}(-\theta_s^{B1}(r)) \begin{pmatrix} \hat{j}_1^{B1} \\ \hat{j}_2^{B1} \\ \hat{j}_3^{B1} \end{pmatrix} \tag{A9}$$

Here, $\theta_s^{B1}(r)$ is the structural twist angle of blade 1. The equations of $\hat{l}^{B2}(r)$ and $\hat{l}^{B3}(r)$ are similar. The blade element fixed coordinate system is given as

$$\begin{pmatrix} \hat{n}_1^{B1}(r) \\ \hat{n}_2^{B1}(r) \\ \hat{n}_3^{B1}(r) \end{pmatrix} = T_O(\theta_x(r), \theta_y(r), 0) \begin{pmatrix} \hat{l}_1^{B1}(r) \\ \hat{l}_2^{B1}(r) \\ \hat{l}_3^{B1}(r) \end{pmatrix} \tag{A10}$$

$\theta_x(r)$ and $\theta_y(r)$ are blade rotations due to elastic deformation in the in-plane and out-of-plane directions respectively at a distance r from the apex of coning angle. The element fixed coordinate system for determining and returning aerodynamic loads are given as

$$\begin{pmatrix} \hat{m}_1^{B1}(r) \\ \hat{m}_2^{B1}(r) \\ \hat{m}_3^{B1}(r) \end{pmatrix} = R_{\hat{n}_3^{B1}}(BlPit(1) + \theta_s^{B1}(r)) \begin{pmatrix} \hat{n}_1^{B1}(r) \\ \hat{n}_2^{B1}(r) \\ \hat{n}_3^{B1}(r) \end{pmatrix} \tag{A11}$$

The equations for $\hat{m}^{B2}(r)$ and $\hat{m}^{B3}(r)$ are similar. When the blades are undeflected, this coordinate system is coincident with $\hat{i}^{B1}$. With all the required coordinate systems defined, the kinematics of the wind turbine is described in the next section.

Appendix B.2. Position Vectors

The position vectors of the various points are listed in this section. The position vector of the tower base (reference point) is given as

$$r^Z = q_{Sq}\hat{z}_1 + q_{Hv}\hat{z}_2 - q_{Sw}\hat{z}_3 \tag{A12}$$

The position vector of the centre of gravity of the platform (Y) from the tower base (Z) is given as

$$r^{ZY} = (PtfmCMzt - PtfmRefzt)\hat{a}_2 \tag{A13}$$

The position vector of tower node at a distance h from tower base is given as

$$\begin{aligned} r^{ZT}(h) = & \left[\phi_1^{TFA}(h)q_{TFA1} + \phi_2^{TFA}(h)q_{TFA2}\right]\hat{a}_1 + \Big[h - 0.5\Big(S_{11}^{TFA}(h)q_{TFA1}^2 + S_{22}^{TFA}(h)q_{TFA2}^2 \\ & + 2S_{12}^{TFA}(h)q_{TFA1}q_{TFA2} + S_{11}^{TSS}(h)q_{TSS1}^2 + S_{22}^{TSS}(h)q_{TSS2}^2 + 2S_{12}^{TSS}(h)q_{TSS1}q_{TSS2}\Big)\Big]\hat{a}_2 \\ & + \left[\phi_1^{TSS}(h)q_{TSS1} + \phi_2^{TFA}(h)q_{TSS2}\right]\hat{a}_3 \end{aligned} \tag{A14}$$

where ϕ_1^{TFA}, ϕ_2^{TFA}, ϕ_2^{TSS} and ϕ_2^{TSS} are the first two mode shapes of the tower in the fore-aft and the side-to-side directions respectively. S_{ij}^{TFA} and S_{ij}^{TSS} are axial deflection shape functions for the tower. The expressions for these quantities are presented in Appendix E. The position vector of tower top/base-plate is given as

$$\begin{aligned} r^{ZO} = & [q_{TFA1} + q_{TFA2}]\hat{a}_1 + \Big[Ht - 0.5\Big(S_{11}^{TFA}(Ht)q_{TFA1}^2 + S_{22}^{TFA}(Ht)q_{TFA2}^2 \\ & + 2S_{12}^{TFA}(Ht)q_{TFA1}q_{TFA2} + S_{11}^{TSS}(Ht)q_{TSS1}^2 + S_{22}^{TSS}(Ht)q_{TSS2}^2 \\ & + 2S_{12}^{TSS}(Ht)q_{TSS1}q_{TSS2}\Big)\Big]\hat{a}_2 + [q_{TSS1} + q_{TSS2}]\hat{a}_3 \end{aligned} \tag{A15}$$

Position vector from the tower-top to the centre of mass of the nacelle is given as

$$r^{OU} = NacCMxn\hat{d}_1 + NacCMzn\hat{d}_2 + NacMyn\hat{d}_3 \tag{A16}$$

Position vector from the tower-top to the apex of coning angle is given as

$$r^{OQ} = OverHang\hat{c}_1 + Twr2Shft\hat{d}_2 - Yaw2Shft\hat{d}_3 \tag{A17}$$

Position vector from the apex of coning angle to the hub centre of mass is given as

$$r^{QC} = HubCM\hat{c}_1 \tag{A18}$$

Position vector from the apex of coning angle to the blade element node for blade 1 is given as

$$
\begin{aligned}
\boldsymbol{r}^{QS1} = {} & \left[\phi_1^{B1}(r) q_{B1F1} + \phi_2^{B1}(r) q_{B1F2} + \phi_3^{B1}(r) q_{B1E1} \right] \hat{\boldsymbol{j}}_1^{B1} + \left[\psi_1^{B1}(r) q_{B1F1} \right. \\
& + \psi_2^{B1}(r) q_{B1F2} + \psi_3^{B1}(r) q_{B1E1} \Big] \hat{\boldsymbol{j}}_2^{B1} + \left[r + HubRad - 0.5 \Big(S_{11}^{B1}(r) q_{B1F1}^2 \right. \\
& + S_{22}^{B1}(r) q_{B1F2} + S_{33}^{B1}(r) q_{B1E1} + 2 S_{12}^{B1}(r) q_{B1F1} q_{B1F2} + 2 S_{13}^{B1}(r) q_{B1F1} q_{B1E1} \\
& + 2 S_{23}^{B1}(r) q_{B1F2} q_{B1E1} \Big) \Big] \hat{\boldsymbol{j}}_3^{B1}
\end{aligned}
\tag{A19}
$$

where $\phi_i(r)$ and $\psi_i(r)$ are the twisted mode shapes in out-of-plane and in-plane directions respectively and S_{ij}^{B1} is the shape of axial deflection. The expression of these quantities are provided in Appendix E. Equations for $\boldsymbol{r}^{QS2}$ and $\boldsymbol{r}^{QS3}$ are similar.

Appendix B.3. Angular Velocities

The angular velocities of various rigid bodies of the wind turbine are defined in the section. The angular velocity of the base of the tower in the inertial (Earth) reference frame is

$$
{}^{E}\boldsymbol{\omega}^{X} = \dot{q}_R \hat{\boldsymbol{z}}_1 + \dot{q}_Y \hat{\boldsymbol{z}}_2 - \dot{q}_P \hat{\boldsymbol{z}}_3
\tag{A20}
$$

The angular velocity of tower node in inertial frame of reference assuming small rotation angles is given as

$$
\begin{aligned}
{}^{E}\boldsymbol{\omega}^{F}(h) = {} & \left[\frac{d\phi_1^{TSS}(h)}{dh} \dot{q}_{TSS1} + \frac{d\phi_2^{TSS}(h)}{dh} \dot{q}_{TSS2} \right] \hat{\boldsymbol{a}}_1 \\
& - \left[\frac{d\phi_1^{TFA}(h)}{dh} \dot{q}_{TFA1} + \frac{d\phi_2^{TFA}(h)}{dh} \dot{q}_{TFA2} \right] \hat{\boldsymbol{a}}_3
\end{aligned}
\tag{A21}
$$

The angular velocity of tower-top in the inertial reference frame is

$$
\begin{aligned}
{}^{E}\boldsymbol{\omega}^{B} = {} & \left[\frac{d\phi_1^{TSS}(h)}{dh} \bigg|_{h=Ht} \dot{q}_{TSS1} + \frac{d\phi_2^{TSS}(h)}{dh} \bigg|_{h=Ht} \dot{q}_{TSS2} \right] \hat{\boldsymbol{a}}_1 \\
& - \left[\frac{d\phi_1^{TFA}(h)}{dh} \bigg|_{h=Ht} \dot{q}_{TFA1} + \frac{d\phi_2^{TFA}(h)}{dh} \bigg|_{h=Ht} \dot{q}_{TFA2} \right] \hat{\boldsymbol{a}}_3
\end{aligned}
\tag{A22}
$$

The angular velocity of the nacelle in the inertial reference frame

$$
{}^{E}\boldsymbol{\omega}^{N} = {}^{E}\boldsymbol{\omega}^{B} + \dot{q}_{yaw} \hat{\boldsymbol{a}}_2
\tag{A23}
$$

The angular velocity of the low speed shaft at the rotor end in inertial reference frame

$$
{}^{E}\boldsymbol{\omega}^{L} = {}^{E}\boldsymbol{\omega}^{N} + \dot{q}_{DrTr} \hat{\boldsymbol{c}}_1 + \dot{q}_{GeAz} \hat{\boldsymbol{c}}_1
\tag{A24}
$$

The angular velocity of blade 1 element in the inertial reference frame

$$
\begin{aligned}
{}^{E}\boldsymbol{\omega}^{M1}(r) = {} & {}^{E}\boldsymbol{\omega}^{L} - \left[\frac{d\psi_1^{B1}(r)}{dr} \dot{q}_{B1F1} + \frac{d\psi_2^{B1}(r)}{dr} \dot{q}_{B1F2} \right. \\
& + \frac{d\psi_3^{B1}(r)}{dr} \dot{q}_{B1E1} \Big] \hat{\boldsymbol{j}}_1^{B1} - \left[\frac{d\phi_1^{B1}(r)}{dr} \dot{q}_{B1F1} \right. \\
& + \frac{d\phi_2^{B1}(r)}{dr} \dot{q}_{B1F2} + \frac{d\phi_3^{B1}(r)}{dr} \dot{q}_{B1E1} \Big] \hat{\boldsymbol{j}}_2^{B1}
\end{aligned}
\tag{A25}
$$

${}^{E}\boldsymbol{\omega}^{M2}(r)$ and ${}^{E}\boldsymbol{\omega}^{M3}(r)$ can be obtained similarly. The generator is connected to the high speed shaft which may or may not rotate in the opposite direction of the low speed shaft

and since q_{GeAz} represents the position of the low speed shaft near the entrance of the gearbox; the angular velocity of the generator is given as

$$^E\boldsymbol{\omega}^G = {}^E\boldsymbol{\omega}^N + GenDir.GBR.\dot{q}_{GeAz}\hat{\boldsymbol{c}}_1 \tag{A26}$$

where *GBR* is the gear box ratio and

$$GenDir = \begin{cases} -1 \text{ for Gear Box Reverse = True} \\ 1 \text{ for Gear Box Reverse = False} \end{cases} \tag{A27}$$

Appendix B.4. Linear Velocities

In this section the linear velocities of all important points of the wind turbine are described. The linear velocity of the tower base can be given as

$$^E\boldsymbol{v}^Z = \dot{q}_{Sq}\hat{\boldsymbol{z}}_1 + \dot{q}_{Hv}\hat{\boldsymbol{z}}_2 - \dot{q}_{Sw}\hat{\boldsymbol{z}}_3 \tag{A28}$$

Linear velocity of tower element in inertial reference frame can be obtained from one point moving on a rigid body formula [27]

$$\begin{aligned} ^E\boldsymbol{v}^T(h) &= {}^E\boldsymbol{v}^Z + {}^E\boldsymbol{v}^{\overline{T}}(h) + {}^X\boldsymbol{v}^T(h) \\ &= {}^E\boldsymbol{v}^Z + {}^E\boldsymbol{\omega}^X(h) \times \boldsymbol{r}^{ZT}(h) + {}^X\boldsymbol{v}^T(h) \end{aligned} \tag{A29}$$

where $^E\boldsymbol{v}^{\overline{T}}$ denotes the velocity in E of the point $\overline{T}$ of X that coincides with T at the instant under consideration. In the above equation $^X\boldsymbol{v}^T$ is given as

$$\begin{aligned} ^X\boldsymbol{v}^T(h) = &\left[\phi_1^{TFA}(h)\dot{q}_{TFA1} + \phi_2^{TFA}(h)\dot{q}_{TFA2}\right]\hat{\boldsymbol{a}}_1 \\ &- \left[S_{11}^{TFA}(h)q_{TFA1}\dot{q}_{TFA1} + S_{22}^{TFA}(h)q_{TFA2}\dot{q}_{TFA2}\right. \\ &+ S_{12}^{TFA}(h)\left(\dot{q}_{TFA1}q_{TFA2} + q_{TFA1}\dot{q}_{TFA2}\right) \\ &+ S_{11}^{TSS}(h)q_{TSS1}\dot{q}_{TSS1} + S_{22}^{TSS}(h)q_{TSS2}\dot{q}_{TSS2} \\ &+ \left. S_{12}^{TSS}(h)\left(\dot{q}_{TSS1}q_{TSS2} + q_{TSS1}\dot{q}_{TSS2}\right)\right]\hat{\boldsymbol{a}}_2 \\ &+ \left[\phi_1^{TSS}(h)\dot{q}_{TSS1} + \phi_2^{TSS}(h)\dot{q}_{TSS2}\right]\hat{\boldsymbol{a}}_3 \end{aligned} \tag{A30}$$

Similarly, the velocity of tower top/base plate can be given as $^X\boldsymbol{v}^O = {}^X\boldsymbol{v}^T(Ht)$. Linear velocity of the nacelle centre of mass can be obtained from two points fixed on a rigid body formula as [27]

$$^E\boldsymbol{v}^U = {}^E\boldsymbol{v}^O + {}^E\boldsymbol{\omega}^N \times \boldsymbol{r}^{OU} \tag{A31}$$

Linear velocity of apex of the coning angle is given as

$$^E\boldsymbol{v}^Q = {}^E\boldsymbol{v}^O + {}^E\boldsymbol{\omega}^L \times \boldsymbol{r}^{OQ} \tag{A32}$$

Linear velocity of centre of mass of hub can be given as

$$^E\boldsymbol{v}^C = {}^E\boldsymbol{v}^Q + {}^E\boldsymbol{\omega}^L \times \boldsymbol{r}^{QC} \tag{A33}$$

Finally, the linear velocity of blade 1 element is given as

$$^E\boldsymbol{v}^{S1}(r) = {}^E\boldsymbol{v}^Q + {}^E\boldsymbol{\omega}^L \times \boldsymbol{r}^{QS1} + {}^L\boldsymbol{v}^{S1}(r) \tag{A34}$$

where

$$
\begin{aligned}
{}^{L}v^{S1}(r) = {} & \left[\phi_1^{B1}(r)\dot{q}_{B1F1} + \phi_2^{B1}\dot{q}_{B1F2} + \phi_3^{B1}\dot{q}_{B1E1} \right]\hat{j}_1^{B1} \\
& + \left[\psi_1^{B1}(r)\dot{q}_{B1F1} + \psi_2^{B1}\dot{q}_{B1F2} + \psi_3^{B1}\dot{q}_{B1E1} \right]\hat{j}_2^{B1} \\
& + \left[S_{11}^{B1}(r)q_{B1F1}\dot{q}_{B1F1} + S_{22}^{B1}(r)q_{B1F2}\dot{q}_{B1F2} \right. \\
& + S_{33}^{B1}(r)q_{B1E1}\dot{q}_{B1E1} + S_{12}^{B1}\left(\dot{q}_{B1F1}q_{B1F2} + q_{B1F1}\dot{q}_{B1F2} \right) + S_{13}^{B1}\left(\dot{q}_{B1F1}q_{B1E1} \right. \\
& + \left. q_{B1F1}\dot{q}_{B1E1} \right) + \left. S_{23}^{B1}\left(\dot{q}_{B1F2}q_{B1E1} + q_{B1F2}\dot{q}_{B1E1} \right) \right]\hat{j}_3^{B1}
\end{aligned}
\tag{A35}
$$

The linear velocities for blade 2, ${}^{E}v^{S2}(r)$ and blade 3, ${}^{E}v^{S3}(r)$ can be obtained similarly.

Appendix B.5. Partial Angular Velocities

According to Kane and Levinson [27], all linear angular velocities can be written as a combination of the partial angular velocities as

$$
{}^{E}\boldsymbol{\omega}^{N_i}(\dot{q},q,t) = \sum_{r=1}^{n} {}^{E}\boldsymbol{\omega}_k^{N_i}(q,t)u_k + {}^{E}\boldsymbol{\omega}_t^{N_i}(q,t)
\tag{A36}
$$

for each rigid body N_i in the system; where n is the number of degrees of freedom in the system and ${}^{E}\omega_k^{N_i}(q,t)$ are the partial angular velocities. u_r are the generalised speeds. In general, u_r are chosen to bring the linear velocities in the above section into particular advantageous form. Here, time derivatives of the DOFs in Equation (1) are chosen as the generalised speeds (i.e., $u_k = \dot{q}_k$). The choice of generalised speeds renders all the ${}^{E}\omega_t^{N_i}(q,t)$ terms as zeros. The angular velocities can be then reorganised to find the partial angular velocity terms ${}^{E}\omega_r^{N_i}$ for every body N_i in the system.

Appendix B.6. Partial Linear Velocities

Similar to partial angular velocities the linear velocities of each point X_i in the system can be written in the form

$$
{}^{E}v^{X_i}(\dot{q},q,t) = \sum_{k=1}^{n} {}^{E}v_k^{X_i}(q,t)u_k + {}^{E}v_t^{X_i}(q,t)
\tag{A37}
$$

where ${}^{E}v_k^{X_i}(q,t)$ are the partial linear velocities. Again, the choice of generalised speeds u_r renders all the ${}^{E}v_t^{N_i}(q,t)$ terms as zeros. The partial linear velocity terms ${}^{E}v_r^{X_i}$ can be obtained from the linear velocities after appropriate arrangement.

Appendix B.7. Angular Accelerations

For every rigid body N_i, in the system the angular acceleration can be obtained from Equation (A36)

$$
{}^{E}\boldsymbol{\alpha}^{N_i} = \sum_{r=1}^{n} {}^{E}\omega_k^{N_i}(q,t)\ddot{q}_k + \sum_{r=1}^{n} \frac{{}^{E}d}{dt}\{{}^{E}\omega_k^{N_i}(q,t)\}\dot{q}_k + \frac{{}^{E}d}{dt}\{{}^{E}\omega_t^{N_i}(q,t)\}
\tag{A38}
$$

In the above expression, $\dfrac{{}^{E}d}{dt}\{{}^{E}\omega_k^{N_i}(q,t)\}$ are the only terms to be evaluated since all other terms are known at this stage. These partial angular acceleration terms can be found using linear velocity relation.

Appendix B.8. Linear Accelerations

Linear accelerator for each point X_i in the system can be obtained from Equation (A37) as

$$^E a^{X_i} = \sum_{r=1}^{n} {}^E v_k^{X_i}(q,t)\ddot{q}_k + \sum_{r=1}^{n} \frac{^E d}{dt}\{{}^E v_k^{X_i}(q,t)\}\dot{q}_k + \frac{^E d}{dt}\{{}^E v_t^{X_i}(q,t)\} \tag{A39}$$

Again, the $\frac{^E d}{dt}\{{}^E v_k^{X_i}\}$ terms are the only required terms as all the other terms are known at this stage.

Appendix C. Kinetics

The kinetic of the FOWT and the resulting equations of motion of the wind turbine system is provided in this section.

Appendix C.1. Platform

The mass of the platform brings about generalised inertia forces. The generalised active forces associated with the platform arise from the gravitational forces, hydrostatic forces, mooring lines and hydrodynamic forces including the effect of added mass. The generalised inertia forces associated with the platform are given as

$$F_r^* \Big|_X = {}^E v_r^Y \cdot (-m^{X\,E} a^Y) + {}^E \omega_r^X \cdot (-{}^E \dot{H}^X) \tag{A40}$$

or

$$F_r^* \Big|_X = {}^E v_r^Y \cdot (-m^{X\,E} a^Y) + {}^E \omega_r^X \cdot (-\bar{\bar{I}}^X \cdot {}^E \alpha^X - {}^E \omega^X \times \bar{\bar{I}}^X \cdot {}^E \omega^X) \tag{A41}$$

where

$$\bar{\bar{I}}^X = PtfrmRIner\,\hat{a}_1\hat{a}_1 + PtfrmYIner\,\hat{a}_2\hat{a}_2 + PtfrmPIner\,\hat{a}_3\hat{a}_3 \tag{A42}$$

Therefore,

$$\begin{aligned}
F_r^* \Big|_X &= {}^E v_r^Y \cdot \Big[-m^X \Big\{ \Big(\sum_{i=1}^{6} {}^E v_i^Y \ddot{q}_i \Big) + \Big(\sum_{i=4}^{6} \frac{dr}{drt}({}^E v_i^Y)\dot{q}_i \Big) \Big\} \Big] \\
&\quad + {}^E \omega_r^X \cdot \Big[-\bar{\bar{I}}^X \cdot \Big(\sum_{i=4}^{6} {}^E \omega_i^X \ddot{q}_i \Big) - {}^E \omega^X \times \bar{\bar{I}}^X \cdot {}^E \omega^X \Big]
\end{aligned} \tag{A43}$$

The elements of the system matrices can be obtained as

$$\begin{aligned}
[\mathbf{M}(\mathbf{q},t)]\Big|_X(k,l) &= m^{X\,E} v_k^Y \cdot {}^E v_l^Y + {}^E \omega_k^X \bar{\bar{I}}^{X\,E} \omega_l^X \quad \text{for } k,l = 1 \text{ to } 6 \\
&= 0 \qquad\qquad\qquad\qquad\qquad\qquad \text{otherwise}
\end{aligned}$$

$$\begin{aligned}
[\mathbf{f}(\dot{\mathbf{q}},\mathbf{q},t)]\Big|_X(k) &= -m^{X\,E} v_k^Y \cdot \Big[\sum_{i=4}^{6} \frac{dr}{drt}({}^E v_i^Y)\dot{q}_i \Big] \\
&\quad - {}^E \omega_k^X \cdot ({}^E \omega^X \times \bar{\bar{I}}^X \cdot {}^E \omega^X) \qquad \text{for } k = 1 \text{ to } 6 \\
&= 0 \qquad\qquad\qquad\qquad\qquad\qquad\qquad \text{otherwise}
\end{aligned} \tag{A44}$$

where the indices k, l are used to denote the row and column respectively of the matrix. Hydrodynamic and hydrostatic forces contribute to the generalised active forces. These forces can be written as

$$F_r \Big|_{HydroX} = {}^E v_k^Y \cdot F_{HydroX}^Y + {}^E \omega_r^X \cdot M_{HydroX}^Y \qquad \text{for } 1 \text{ to } 22 \tag{A45}$$

where F_{HydroX}^Y and M_{HydroX}^Y are the forces and moments acting at the platform centre of mass. These forces can be transformed to forces at the base of the wind turbine as

$$F_{HydroX}^Z = F_{HydroX}^Y \tag{A46}$$

and

$$M_{HydroX}^Y = M_{HydroX}^Z + r^{YZ} \times F_{HydroX}^Z = M_{HydroX}^Z - r^{ZY} \times F_{HydroX}^Z \tag{A47}$$

However, since, ${}^E v_r^Y = {}^E v_r^Z + {}^E \omega_r^X \times r^{ZY}$, the generalised active forces can be written as

$$F_r\Big|_{HydroX} = \left[{}^E v_r^Z + {}^E \omega_r^X \times r^{ZY} \right] \cdot F_{HydroX}^Z + {}^E \omega_r^X \cdot \left[M_{HydroX}^Z - r^{ZY} \times F_{HydroX}^Z \right] \tag{A48}$$
$$\text{for 1 to 22}$$

This simplifies to

$$F_r\Big|_{HydroX} = {}^E v_k^Z \cdot F_{HydroX}^Z + {}^E \omega_r^X \cdot M_{HydroX}^Z \qquad \text{for 1 to 22} \tag{A49}$$

Other than the motion of the liquid the hydrodynamic forces and moments also depend on the motion of the platform. The forces and moments can be written as

$$F_{HydroX}^Z = \left(\sum_{i=1}^{6} F_{HydroX_j}^Z \ddot{q}_j \right) + F_{HydroX_t}^Z \tag{A50}$$

and

$$M_{HydroX}^Z = \left(\sum_{i=1}^{6} M_{HydroX_j}^Z \ddot{q}_j \right) + M_{HydroX_t}^Z \tag{A51}$$

where $F_{HydroX_t}^Z$ and $M_{HydroX_t}^Z$ are the hydrodynamic forces and moments that do not depend of the acceleration of the platform. Thus,

$$F_r\Big|_{HydroX} = {}^E v_k^Z \cdot \left[\left(\sum_{i=1}^{6} F_{HydroX_j}^Z \ddot{q}_j \right) + F_{HydroX_t}^Z \right]$$
$$+ {}^E \omega_r^X \cdot \left[\left(\sum_{i=1}^{6} M_{HydroX_j}^Z \ddot{q}_j \right) + M_{HydroX_t}^Z \right] \qquad \text{for } r = 1 \text{ to } 22 \tag{A52}$$

Finally, the system matrices can be obtained as

$$[\mathbf{M}(\mathbf{q}, t)]\Big|_{HydroX}(k, l) = -{}^E v_k^Z \cdot F_{HydroX_l}^Z - {}^E \omega_k^X \cdot M_{HydroX_l}^Z \quad k, l = 1 \text{ to } 6$$
$$= 0 \qquad\qquad\qquad \text{otherwise}$$
$$f(\dot{q}, q, t)\Big|_{HydroX}(k) = {}^E v_k^Z \cdot F_{HydroX_t}^Z + {}^E \omega_k^X \cdot M_{HydroX_t}^Z \qquad k = 1 \text{ to } 6$$
$$= 0 \qquad\qquad\qquad \text{otherwise} \tag{A53}$$

Gravitational force contribute to the generalised active forces on the platform. These forces can be written as

$$F_r\Big|_{GravX} = {}^E v_k^Y \cdot (-m^X g \hat{z}_2) \tag{A54}$$

where g is acceleration due to gravity. The system matrices can be obtained as

$$
\begin{aligned}
[\mathbf{M}(\mathbf{q},t)]\Big|_{GravX}(k,l) &= 0 & \text{for all} \\
f(\dot{q},q,t)\Big|_{GravX}(k) &= -m^X g^E v_k^Y \cdot \hat{z}_2 & k = 1 \text{ to } 6 \\
&= 0 & \text{otherwise}
\end{aligned}
\tag{A55}
$$

Appendix C.2. Tower

The distributed sectional properties of the tower bring about generalised active and inertia forces and associated with tower elasticity, damping, aerodynamics and mass. The generalised inertial forces associated with the tower mass can be obtained as [64]

$$
\begin{aligned}
F_k^*\Big|_T &= -\int_0^{Ht} \mu^T(h)^E v_k^T(h) \cdot {}^E a^T(h)dh \\
&\quad - YBMass.{}^E v_k^O \cdot {}^E a^O \quad \text{for } k = 1 \text{ to } 10
\end{aligned}
\tag{A56}
$$

where $YBMass$ is the yaw bearing mass. Using the expression for the partial linear velocities and acceleration of tower nodes the elements of the system matrices can be found as

$$
\begin{aligned}
[\mathbf{M}(\mathbf{q},t)]\Big|_T(k,l) &= \int_0^{Ht} \mu^T(h)^E v_k^T(h) \cdot {}^E v_l^T(h)dh \\
&\quad + YBMass.{}^E v_k^O \cdot {}^E v_l^O & \text{for } k,l = 1 \text{ to } 10 \\
&= 0 & \text{otherwise} \\
\{-f(\dot{q},q,t)\}\Big|_T(k) &= -\int_0^{Ht} \mu^T(h)^E v_k^T(h) \cdot \left(\sum_{i=1}^{4} \frac{d}{dt}\{^E v_i^T(h)\}\dot{q}_i \right)dh \\
&\quad - YBMass.{}^E v_k^O \cdot \left(\sum_{i=1}^{4} \frac{d}{dt}\{^E v_i^O\}\dot{q}_i \right) & \text{for } k = 1 \text{ to } 10 \\
&= 0 & \text{otherwise}
\end{aligned}
\tag{A57}
$$

where the indices k, l are used to denote the row and column respectively of the matrix. Generalised active forces arise from the elasticity and damping of the flexible members. The generalised elastic forces can be obtained from the potential energy stored in the member as

$$
F_k\Big|_{ElasticT} = \frac{\partial V^T}{\partial q_k} \quad \text{for } k = 1 \text{ to } 10
\tag{A58}
$$

$$
\{-f(\dot{q},q,t)\}\Big|_T(k) = F_k\Big|_{ElasticT} =
\begin{cases}
-k_{11}^{TFA}q_{TFA1} - k_{12}^{TFA}q_{TFA2} & \text{for } k = 7 \\
-k_{11}^{TSS}q_{TSS1} - k_{12}^{TSS}q_{TSS2} & \text{for } k = 8 \\
-k_{21}^{TFA}q_{TFA1} - k_{22}^{TFA}q_{TFA2} & \text{for } k = 9 \\
-k_{21}^{TSS}q_{TSS1} - k_{22}^{TFA}q_{TSS2} & \text{for } k = 10 \\
0 & \text{otherwise}
\end{cases}
\tag{A59}
$$

where k_{ij}^{TFA} and k_{ij}^{TSS} are the generalised stiffness of the tower in the fore-aft and side-to-side directions respectively when gravitational de-stiffening effects are not included

$$
\begin{aligned}
k_{ij}^{TFA} &= \int_0^{Ht} EI^{TFA}(h)\frac{d^2\phi_i^{TFA}}{dh^2}\frac{d^2\phi_j^{TFA}}{dh^2}dh \quad \text{for } i,j = 1,2 \\
k_{ij}^{TSS} &= \int_0^{Ht} EI^{TSS}(h)\frac{d^2\phi_i^{TSS}}{dh^2}\frac{d^2\phi_j^{TSS}}{dh^2}dh \quad \text{for } i,j = 1,2
\end{aligned}
\tag{A60}
$$

Using Rayleigh damping technique where the damping is assumed proportional to the stiffness, the generalised active forces can be obtained as

$$
\{-f(\dot{q}, q, t)\}\Big|_T(k) = F_k\Big|_{DampT} = \begin{cases} -\dfrac{\zeta_1^{TFA} k_{11}^{TFA}}{\pi f_1^{TFA}}\dot{q}_{TFA1} - \dfrac{\zeta_2^{TFA} k_{12}^{TFA}}{\pi f_2^{TFA}}\dot{q}_{TFA2} & \text{for } k = 7 \\[2ex] -\dfrac{\zeta_1^{TSS} k_{11}^{TSS}}{\pi f_1^{TSS}}\dot{q}_{TSS1} - \dfrac{\zeta_2^{TSS} k_{12}^{TSS}}{\pi f_2^{TSS}}\dot{q}_{TSS2} & \text{for } k = 8 \\[2ex] -\dfrac{\zeta_1^{TFA} k_{21}^{TFA}}{\pi f_1^{TFA}}\dot{q}_{TFA1} - \dfrac{\zeta_2^{TFA} k_{22}^{TFA}}{\pi f_2^{TFA}}\dot{q}_{TFA2} & \text{for } k = 9 \\[2ex] -\dfrac{\zeta_1^{TSS} k_{21}^{TFA}}{\pi f_1^{TSS}}\dot{q}_{TSS1} - \dfrac{\zeta_2^{TFA} k_{22}^{TSS}}{\pi f_2^{TSS}}\dot{q}_{TSS2} & \text{for } k = 10 \\[2ex] 0 & \text{otherwise} \end{cases} \quad \text{(A61)}
$$

where ζ_i^{TFA} and ζ_i^{TSS} represents the structural damping ratio of the tower for the *i*th mode in the fore-aft and side-to-side direction respectively. Futhermore, f_i^{TFA} and f_i^{TSS} represent the natural frequency of the tower for the *i*th mode of the tower in the fore-aft and side-to-side directions respectively without the tower-top mass or gravitational de-stiffening effects. Gravitation forces on the tower contribute to the generalised active force as

$$
F_k\Big|_{GravT} = \int_0^{Ht} {}^E v_k^T(h) \cdot \{-\mu_T(h)g\hat{z}_2\}dh \\
- YBMass.g.{}^E v_k^O \cdot \hat{z}_2 \quad \text{for } k = 1 \text{ to } 10 \quad \text{(A62)}
$$

Thus,

$$
[\mathbf{M}(\mathbf{q}, t)]\Big|_{GravT}(k, l) = 0 \qquad\qquad \text{for all}
$$
$$
\{-f(\dot{q}, q, t)\}\Big|_{GravT}(k) = -\int_0^{Ht} {}^E v_k^T(h) \cdot \{\mu_T(h)g\hat{z}_2\}dh \\
- YBMass.g.{}^E v_k^O \cdot \hat{z}_2 \qquad \text{for } k = 1 \text{ to } 10 \quad \text{(A63)} \\
= 0 \qquad\qquad \text{otherwise}
$$

Aerodynamic forces on the tower contribute to the generalised active force as

$$
F_k\Big|_{AeroT} = \int_0^{Ht} \left[{}^E v_k^T(h) \cdot \mathbf{F}_{AeroT}^T(h) + {}^E \omega_k^F(h) \cdot \mathbf{M}_{AeroT}^F(h) \right]dh \qquad \text{for } k = 1 \text{ to } 10 \quad \text{(A64)}
$$

where $\mathbf{F}_{AeroT}^T(h)$ and $\mathbf{M}_{AeroT}^F(h)$ are aerodynamic forces and moments applied on the tower expressed per unit length. Thus,

$$
[\mathbf{M}(\mathbf{q}, t)]\Big|_{AeroT}(k, l) = 0 \qquad\qquad \text{for all}
$$
$$
\{-f(\dot{q}, q, t)\}\Big|_{GravT}(k) = \int_0^{Ht} \left[{}^E v_k^T(h) \cdot \mathbf{F}_{AeroT}^T(h) \right. \\
\left. + {}^E \omega_k^F(h) \cdot \mathbf{M}_{AeroT}^F(h) \right]dh \qquad \text{for } k = 1 \text{ to } 10 \quad \text{(A65)} \\
= 0 \qquad\qquad \text{otherwise}
$$

Appendix C.3. Yaw Bearing

The yaw spring and damper bring about generalised active forces. The generalised active force from the yaw spring

$$
F_r\Big|_{YawSpr} = \begin{cases} -YawSpr.(q_{yaw} - q_{yaw_0}) & \text{for } k = 11 \\ 0 & \text{otherwise} \end{cases} \quad \text{(A66)}
$$

where q_{yaw_0} is the initial neutral position of the yaw bearing. Futhermore, the generalised active force from the yaw damper

$$F_r\Big|_{YawDamp} = \begin{cases} -YawDamp.\dot{q}_{yaw} & \text{for } k = 11 \\ 0 & \text{otherwise} \end{cases} \tag{A67}$$

Thus,

$$[\mathbf{M}(\mathbf{q},t)]\Big|_{YawBear}(k,l) = 0 \qquad\qquad \text{for all}$$

$$\{-f(\dot{q},q,t)\}\Big|_{YawBear}(k) = -YawSpr.(q_{yaw} - q_{yaw_0})$$
$$- YawDamp.\dot{q}_{yaw} \qquad \text{for } k = 11$$
$$= 0 \qquad\qquad \text{otherwise} \tag{A68}$$

Appendix C.4. Nacelle

The rigid lump mass of the nacelle brings about generalised inertia forces and generalised active forces associated with nacelle weight. Generalised inertia forces can be given as

$$F_r^*\Big|_N = {}^E v_r^U \cdot \left(-m^N {}^E a^U\right) - {}^E \omega_r^N \cdot \left(\bar{\bar{I}}^N \cdot {}^E \alpha^N + {}^E \omega^N \times \bar{\bar{I}}^N \cdot {}^E \omega^N\right) \quad \text{for } r = 1 \text{ to } 11 \tag{A69}$$

where m^N is the nacelle mass and the inertia dyadic can be given as

$$\bar{\bar{I}}^N = \left[NacYIner - m^N\left(NacCMxn^2 + NacCMyn^2\right)\right]\hat{d}_2\hat{d}_2 \tag{A70}$$

using parallel axis theorem. Using the expressions for partial linear velocities, acceleration and rate of change of angular momentum of the nacelle the system matrices can be obtained as Thus,

$$[\mathbf{M}(\mathbf{q},t)]\Big|_N(k,l) = m^N {}^E v_k^U \cdot {}^E v_l^U + {}^E \omega_k^N \cdot \bar{\bar{I}}^N \cdot {}^E \omega_l^N \quad \text{for } k,l = 1 \text{ to } 11$$
$$= 0 \qquad\qquad \text{otherwise}$$

$$\{-f(\dot{q},q,t)\}\Big|_N(k) = -m^N {}^E v_k^U \cdot \sum_{i=1}^{5} \frac{d}{dt}\left({}^E v_i^U\right)\dot{q}_i$$
$$- {}^E \omega_k^N \cdot \left[-\bar{\bar{I}}^N \cdot \left\{\sum_{i=1}^{5} \frac{d}{dt}\left({}^E \omega_i^N\right)\dot{q}_i\right\}\right.$$
$$\left. - {}^E \omega^N \times \bar{\bar{I}}^N \cdot {}^E \omega^N\right] \qquad \text{for } k = 1 \text{ to } 11$$
$$= 0 \qquad\qquad \text{otherwise} \tag{A71}$$

The generalised active force brought about by the gravitational force is given as

$$F_k\Big|_N = {}^E v_k^U \cdot \left(-m^N g \hat{z}_2\right) \quad \text{for } k = 1 \text{ to } 11 \tag{A72}$$

Thus,

$$[\mathbf{M}(\mathbf{q},t)]\Big|_{GravN}(k,l) = 0 \qquad\qquad \forall\, k,l$$

$$\{-f(\dot{q},q,t)\}\Big|_{GravN}(k) = {}^E v_k^U \cdot \left(-m^N g \hat{z}_2\right) \quad \text{for } k = 1 \text{ to } 11$$
$$= 0 \qquad\qquad \text{otherwise} \tag{A73}$$

Appendix C.5. Hub

The rigid lump mass of the hub brings about generalised inertia forces and generalised active forces associated with the hub weight. Generalised inertia forces are given as

$$\left. F_r^* \right|_H = {}^E v_r^C \cdot \left(-m^{H\,E} a^C \right) - {}^E \omega_r^H \cdot \left(\bar{\bar{I}}^H \cdot {}^E \alpha^H + {}^E \omega^H \times \bar{\bar{I}}^H \cdot {}^E \omega^H \right) \quad \text{for } r = 1 \text{ to } 13 \quad \text{(A74)}$$

where m^H is the hub mass and the inertia dyadic can be given as

$$\bar{\bar{I}}^H = \left[HubIner - m^H \left(HubCM^2 \right) \right] \hat{e}_1 \hat{e}_1 \quad \text{(A75)}$$

using parallel axis theorem. Using the expressions for partial linear velocities, acceleration and rate of change of angular momentum of the hub the system matrices can be obtained as Thus,

$$\left. [\mathbf{M}(\mathbf{q}, t)] \right|_H (k, l) = m^{H\,E} v_k^C \cdot {}^E v_l^C + {}^E \omega_k^H \cdot \bar{\bar{I}}^H \cdot {}^E \omega_l^H \quad \text{for } k, l = 1 \text{ to } 13$$

$$= 0 \quad \text{otherwise}$$

$$\left. \{ -f(\dot{q}, q, t) \} \right|_H (k) = -m^{H\,E} v_k^C \cdot \sum_{i=1}^{7} \frac{d}{dt} ({}^E v_i^C) \dot{q}_i$$

$$- {}^E \omega_k^H \cdot \left[-\bar{\bar{I}}^H \cdot \left\{ \sum_{i=1}^{7} \frac{d}{dt} ({}^E \omega_i^H) \dot{q}_i \right\} \right.$$

$$\left. - {}^E \omega^H \times \bar{\bar{I}}^H \cdot {}^E \omega^H \right] \quad \text{for } k = 1 \text{ to } 13$$

$$= 0 \quad \text{otherwise}$$

(A76)

The generalised active force brought about by the gravitational force is given as

$$\left. F_k \right|_{GravH} = {}^E v_k^C \cdot \left(-m^H g \hat{z}_2 \right) \quad \text{for } k = 1 \text{ to } 13 \quad \text{(A77)}$$

Thus,

$$\left. [\mathbf{M}(\mathbf{q}, t)] \right|_{GravH} (k, l) = 0 \quad \text{for all}$$

$$\left. \{ -f(\dot{q}, q, t) \} \right|_{GravH} (k) = {}^E v_k^C \cdot \left(-m^H g \hat{z}_2 \right) \quad \text{for } k = 1 \text{ to } 7$$

$$= 0 \quad \text{otherwise}$$

(A78)

Appendix C.6. Blades

The distributed properties of blade 1 brings about generalised inertia forces and generalised active forces associated with blade elasticity, damping, weight and aerodynamic loads. Generalised inertia forces can be given as

$$\left. F_k^* \right|_{B1} = -\int_0^{BlLn} \mu^{B1}(r) {}^E v_k^{S1}(r) \cdot {}^E a^{S1}(r) dr \quad \text{for } k = 1 \text{ to } 16 \quad \text{(A79)}$$

Thus, using the partial linear velocities and acceleration of the blade nodes the system matrices can be found as

$$\left. [\mathbf{M}(\mathbf{q},t)] \right|_{B1}(k,l) = \int_0^{BlLn} \mu^{B1}(r)\,^E v_k^{S1}(r) \cdot\,^E v_l^{S1}(r)\,dr \qquad \text{for } k,l = 1 \text{ to } 16$$

$$= 0 \qquad\qquad\qquad \text{otherwise}$$

$$\left. \{-f(\dot{q},q,t)\} \right|_{B1}(k) = -\int_0^{BlLn} \mu^{B1}(r)\,^E v_k^{S1}(r) \cdot \left(\sum_{i=1}^{10} \frac{d}{dt}\{^E v_i^{S1}(r)\}\dot{q}_i \right) dr \qquad \text{for } k = 1 \text{ to } 16$$

$$= 0 \qquad\qquad\qquad \text{otherwise} \tag{A80}$$

The generalised elastic forces can be obtained from the potential energy stored in the member as

$$\left. F_k \right|_{ElasticB1} = \frac{\partial V^{B1}}{\partial q_k} \quad \text{for } k = 1 \text{ to } 16 \tag{A81}$$

$$\left. \{-f(\dot{q},q,t)\} \right|_{ElasticB1}(k) = \left. F_k \right|_{ElasticB1} = \begin{cases} -k_{11}^{B1F}q_{B1F1} - k_{12}^{B1F}q_{B1F2} & \text{for } k = 14 \\ -k_{11}^{B1E}q_{B1E1} & \text{for } k = 15 \\ -k_{22}^{B1F}q_{B1F2} - k_{21}^{B1F}q_{B1F1} & \text{for } k = 16 \\ 0 & \text{otherwise} \end{cases} \tag{A82}$$

where k_{ij}^{B1F} and k_{ij}^{B1E} are the generalised stiffness of the blade in the local flapwise and edgewise directions respectively when gravitational de-stiffening and centrifugal stiffening effects are not included

$$k_{ij}^{B1F} = \int_0^{BlLn} EI^{B1F}(r)\left[\frac{d^2\phi_i^{B1F}(r)}{dr^2}\right]\left[\frac{d^2\phi_j^{B1F}(r)}{dr^2}\right]dr \quad i,j = 1,2$$

$$k_{11}^{B1E} = \int_0^{BlLn} EI^{B1E}(r)\left[\frac{d^2\phi_1^{B1E}(r)}{dr^2}\right]^2 dr \tag{A83}$$

Using Rayleigh damping technique where the damping is assumed proportional to the stiffness, the generalised active forces arising from the damping in the member can be obtained as

$$\left. \{-f(\dot{q},q,t)\} \right|_{DampB1}(k) = \left. F_k \right|_{DampB1} =$$

$$\begin{cases} -\dfrac{\zeta_1^{B1F}k_{11}^{B1F}}{\pi f_1^{B1F}}\dot{q}_{B1F1} - \dfrac{\zeta_2^{B1F}k_{22}^{B1F}}{\pi f_2^{B1F}}\dot{q}_{B1F2} & \text{for } k = 14 \\ -\dfrac{\zeta_1^{B1E}k_{11}^{B1E}}{\pi f_1^{B1E}}\dot{q}_{B1E1} & \text{for } k = 15 \\ -\dfrac{\zeta_1^{B2F}k_{22}^{B1F}}{\pi f_2^{B1F}}\dot{q}_{B1F2} - \dfrac{\zeta_1^{B1F}k_{11}^{B1F}}{\pi f_1^{B1F}}\dot{q}_{B1F1} & \text{for } k = 16 \\ 0 & \text{otherwise} \end{cases} \tag{A84}$$

where ζ_i^{B1F} and ζ_i^{B1E} represents the structural damping ratio of the blade in the flapwise and edgewise directions respectively. Futhermore, f_i^{B1F} and f_i^{B1E} represent the natural frequency of the blade for the first mode in the flapwise and edgewise directions respectively without the centrifugal stiffening or gravitational de-stiffening effects. Gravitational forces on the blades contribute to the generalised active force as

$$\left. F_k \right|_{GravB1} = \int_0^{BlLn}\,^E v_k^{S1}(r) \cdot \{-\mu_{B1}(r)g\hat{z}_2\}\,dr \qquad \text{for } k = 1 \text{ to } 16 \tag{A85}$$

Thus,

$$\left[\mathbf{M}(\mathbf{q},t)\right]\Big|_{GravB1}(k,l) = 0 \qquad \text{for all}$$

$$\left\{-f(\dot{q},q,t)\right\}\Big|_{GravB1}(k) = -\int_0^{BlLn} {}^E v_k^{S1}(r) \cdot \{\mu_{B1}(r)g\hat{z}_\mathbf{2}\}dh \quad \text{for } k = 1 \text{ to } 10 \qquad \text{(A86)}$$

$$= 0 \qquad \text{otherwise}$$

Aerodynamic forces on the blades contribute to the generalised active force as

$$F_k\Big|_{AeroB1} = \int_0^{BlLn} \left[{}^E v_k^{S1}(r) \cdot F_{AeroB1}^{S1}(r) + {}^E \omega_k^{M1}(r) \cdot M_{AeroB1}^{M1}(r)\right]dr \qquad \text{for } k = 1 \text{ to } 16 \qquad \text{(A87)}$$

where $F_{AeroB1}^{S1}(r)$ and $M_{AeroB1}^{M1}(r)$ are aerodynamic forces and pitching moments per unit length on the blade receptively. $M_{AeroB1}^{M1}(r)$ can include effect of both direct aerodynamic pitching moments and aerodynamic pitching moments caused by an aerodynamic offset (i.e., moments due to aerodynamic lift and drag acting at a distance away from the centre of mass of the blade element along the aerodynamic cord). Thus, using the partial angular and linear velocities of the blade nodes

$$\left[\mathbf{M}(\mathbf{q},t)\right]\Big|_{AeroB1}(k,l) = 0 \qquad \forall\, k,l$$

$$\{-f(\dot{q},q,t)\}\Big|_{AeroB1}(k) = \int_0^{BlLn} \left[{}^E v_r^{S1}(r) \cdot F_{AeroB1}^{S1}(r) \right.$$

$$\left. + {}^E \omega_r^{M1}(r) \cdot M_{AeroB1}^{M1}(r)\right]dr \qquad \text{for } k = 1 \text{ to } 10 \qquad \text{(A88)}$$

$$= 0 \qquad \text{otherwise}$$

Similar to blade 1, the distributed properties of blade 2 and blade 3 bring about generalised inertia forces and active forces associated with blade elasticity, blade damping, blade weight, and aerodynamic loads. The equations for $F_k^*\Big|_{B2}$, $F_k^*\Big|_{B3}$, $F_k\Big|_{ElasticB2}$, $F_k\Big|_{ElasticB3}$, $F_k\Big|_{DampB2}$, $F_k\Big|_{DampB3}$, $F_k\Big|_{GravB2}$, $F_k\Big|_{GravB3}$, $F_k\Big|_{AeroB2}$ and $F_k\Big|_{AeroB3}$ can be found similarly.

Appendix C.7. Drivetrain

The inertia of the drivetrain brings about generalised inertia forces and the load in the generator, high speed shaft brake and the flexibility of the low speed shaft bring about generalised active forces. Note that it is assumed that the rotor is spinning about positive $\hat{c}$ axis. This is a simply gearbox model which assumes that the gearbox rotates about the shaft axis (i.e., the gear box may not be skewed with respect to the shaft) and there is no friction forces between in the gear box. If there is no gearbox, $GBR = GenDir = 1$. The mechanical torque within the generator is applied to the high speed shaft equally and oppositely to the structure that rotates with the rotor

$$F_k\Big|_{Gen} = \left({}^E \omega_k^G - {}^E \omega_k^N\right) \cdot M_{Gen}^G \quad \text{for } k = 1 \text{ to } 12 \qquad \text{(A89)}$$

Thus,

$$F_k\Big|_{Gen} = \begin{cases} {}^E \omega_{GeAz}^G \cdot M_{Gen}^G & \text{for } k = GeAz \\ 0 & \text{otherwise} \end{cases} \qquad \text{(A90)}$$

where the mechanical torque can be given as

$$M_{Gen}^G = -GenDir.T^{Gen}(GBR.\dot{q}_{GeAz},t)\hat{c}_\mathbf{1} \qquad \text{(A91)}$$

A positive T^{Gen} represents a load (positive power extracted) whereas a negative T^{Gen} represents a motoring-up (negative power extracted or power input). Thus,

$$F_k\Big|_{Gen} = \begin{cases} -GBR.T^{Gen}(GBR.\dot{q}_{GeAz}, t) & \text{for } k = GeAz \\ 0 & \text{otherwise} \end{cases} \tag{A92}$$

And,

$$[\mathbf{M}(\mathbf{q}, t)]\Big|_{Gen}(k, l) = 0 \qquad\qquad \text{for all}$$

$$\{-f(\dot{q}, q, t)\}\Big|_{Gen}(k) = -GBR.T^{Gen}(GBR.\dot{q}_{GeAz}, t) \quad \text{for } k = 12$$

$$= 0 \qquad\qquad \text{otherwise} \tag{A93}$$

The transnational inertia of the drivetrain is to be incorporated into the structure that rotates with the nacelle, then the high speed shaft generator inertia generalised force is given as

$$F_r^*\Big|_G = -{}^E\boldsymbol{\omega}_r^G \cdot \left(\bar{\bar{\boldsymbol{I}}}^G \cdot {}^E\boldsymbol{\alpha}^G + {}^E\boldsymbol{\omega}^G \times \bar{\bar{\boldsymbol{I}}}^G \cdot {}^E\boldsymbol{\omega}^G \right) \quad \text{for } r = 1 \text{ to } 12 \tag{A94}$$

where the inertia dyadic can be given as

$$\bar{\bar{\boldsymbol{I}}}^G = GenIner\,\hat{c}_1\hat{c}_1 \tag{A95}$$

The terms associated with DOFs 1 to 12 represent the fact that the rate of change of angular momentum of the generator can be considered as an additional torque on the structure that rotates with the nacelle (i.e., in addition to the torque on the structure transmitted from the low speed shaft). After some mathematical manipulation

$$[\mathbf{M}(\mathbf{q}, t)]\Big|_G(k, l) = {}^E\boldsymbol{\omega}_k^G \cdot \bar{\bar{\boldsymbol{I}}}^G \cdot {}^E\boldsymbol{\omega}_l^G \qquad\qquad \text{for } k, l = 1 \text{ to } 12$$

$$= 0 \qquad\qquad\qquad \text{otherwise}$$

$$\{-f(\dot{q}, q, t)\}\Big|_G(k) = -{}^E\boldsymbol{\omega}_k^G \cdot \left[\bar{\bar{\boldsymbol{I}}}^G \cdot \left\{ \sum_{i=1}^5 \frac{d}{dt}({}^E\boldsymbol{\omega}_i^N)\dot{q}_i \right\} \right.$$

$$\left. + {}^E\boldsymbol{\omega}^G \times \bar{\bar{\boldsymbol{I}}}^G \cdot {}^E\boldsymbol{\omega}^G \right] \qquad\qquad \text{for } k = 1 \text{ to } 11 \tag{A96}$$

$$= -{}^E\boldsymbol{\omega}_k^G \cdot \bar{\bar{\boldsymbol{I}}}^G \cdot \left\{ \sum_{i=1}^5 \frac{d}{dt}({}^E\boldsymbol{\omega}_i^N)\dot{q}_i \right\} \qquad \text{for } k = 12$$

$$= 0 \qquad\qquad\qquad \text{otherwise}$$

The elasticity of the low speed shaft brings about generalised active force which can be obtained as

$$F_k\Big|_{ELasticDrive} = \frac{\partial V_{Drive}}{\partial q_k} \quad \text{for } k = 1 \text{ to } 12 \tag{A97}$$

where V_{Drive} is the potential energy in the drivetrain given as $\frac{1}{2}DTTorSpr.q_{DrTr}^2$. Hence,

$$[\mathbf{M}(\mathbf{q}, t)]\Big|_{DriveTrain}(k, l) = 0 \qquad \text{for all} \tag{A98}$$

and

$$\{-f(\dot{q}, q, t)\}\Big|_G(k) = F_r\Big|_{ELasticDrive} = \begin{cases} -DTTorSpr.q_{DrTr} & \text{for } k = 12 \\ 0 & \text{otherwise} \end{cases} \tag{A99}$$

Likewise, the contribution of damping to the generalised active forces can be written as

$$\left.\{-f(\dot{q},q,t)\}\right|_G (k) = \left.F_r\right|_{DampDrive} = \begin{cases} -DTTorDmp.\dot{q}_{DrTr} & \text{for } k = 12 \\ 0 & \text{otherwise} \end{cases} \tag{A100}$$

Here, it must be noted that the mechanical friction in the gearbox will exert a torque on the high speed shaft. In this study, the mechanical friction torque is neglected and it is assumed that the gearbox operates with 100% efficiency.

The final equations of motion of the system are obtained by assembling the contribution from every component to form the final $[\mathbf{M}(\mathbf{q},t)]$ and $\{-f(\dot{q},q,t)\}$ matrices. It is worth noting here that terms in $[\mathbf{M}(\mathbf{q},t)]$ and $\{-f(\dot{q},q,t)\}$ can be evaluated directly using a computer and a priori closed form knowledge of equations of motion are not required. This has a particular advantage for complex structures with large numbers of components and reference frames which makes the evaluation of closed form equations practically impossible.

Appendix D. Coupling TMDI to FOWT

This section provides the kinematics, kinetics and system matrices of the TMDI couple to the wind turbine tower.

Appendix D.1. Position Vector

Position vector from tower top to the centre of mass of the TMD denoted by the point D is defined as

$$r^{OD} = \begin{cases} h_{TMDI}\hat{d}_2 + q_{TMDI}\hat{d}_3 & \text{for side-to-side coupling} \\ h_{TMDI}\hat{d}_2 + q_{TMDI}\hat{d}_1 & \text{for fore-aft coupling} \end{cases} \tag{A101}$$

where h_{TMDI} is the vertical distance of the TMD centre of mass from tower top and q_{TMDI} is the new generalised coordinate that describes the motion of the TMDI mass in the nacelle coordinate system along $\hat{d}_3$ when coupled to the side-to-side direction and along $\hat{d}_1$ when coupled to the fore-aft direction.

Appendix D.2. Linear Velocity Vector

The linear velocity vector of the TMDI mass can be obtained as

$$^E v^D = {}^E v^O + {}^N v^D + {}^E \omega^N \times r^{OD} \tag{A102}$$

Appendix D.3. Partial Linear Velocities

The linear velocity of the TMD can be rearranged to obtained the partial linear velocities

$$^E v_k^D = {}^E v_k^O + \begin{cases} ^E \omega_k^N \times r^{OD} & \text{for } k = 1 \text{ to } 11 \\ \hat{d}_3 \text{ or } \hat{d}_1 & \text{for } k = 23 \\ 0 & \text{otherwise} \end{cases} \tag{A103}$$

$$^E v_t^D = 0$$

Appendix D.4. Linear Accelerations

Lastly, the acceleration of the TMD mass is written in terms of partial linear acceleration as

$$^E a^D = \sum_{k=1}^n {}^E v_k^D \ddot{q}_k + \sum_{k=1}^n \frac{^E d}{dt}({}^E v_k^D)\dot{q}_k + \frac{^E d}{dt}\{{}^E v_t^{D_i}(q,t)\} \tag{A104}$$

Similar to the previous section, the only terms to be estimated are $\frac{^Ed}{dt}(^Ev_k^D)$ as the rest of the terms are known at this stage.

Appendix D.5. Kinetics and Kane's Equations of Motion

　　The TMDI will bring about generalised active and inertial forces will can be summed up with the generalised active and inertial forces of the wind turbine to obtain the coupled equations of motion.

　　Generalised inertial forces can be given as

$$F_k^*\Big|_{TMDI} = {}^Ev_k^D \cdot (-m_{TMDI}{}^Ea^D) \tag{A105}$$

The system matrices are obtained as

$$[\mathbf{M}(\mathbf{q},t)]\Big|_{TMDI}(k,l) = m_{TMDI}{}^Ev_k^D \cdot {}^Ev_l^D \qquad \text{for } k,l = 1 \text{ to } 11, 23$$

$$\{-f(\dot{q},q,t)\}\Big|_{TMDI}(k) = -m_{TMDI}{}^Ev_k^D \cdot \left[\sum_{i=1}^{11} \frac{d}{dt}(^Ev_i^D)\dot{q}_i \right. \tag{A106}$$

$$\left. + \frac{d}{dt}(^Ev_{TMDI}^D)\dot{q}_{TMDI} \right] \qquad \text{for } k,l = 1 \text{ to } 11, 23$$

The inerter force brings about generalised active forces on the damper and the tower as

$$\{-f(\dot{q},q,t)\}\Big|_{TMDIInerter}(k) = {}^Ev_k^D \cdot \left\{ -b\left[{}^Ea^D - {}^Ea^T(H_I)\right] \right\} \qquad \text{for } k = 1 \text{ to } 11, 23 \tag{A107}$$

and

$$\{-f(\dot{q},q,t)\}\Big|_{TwrInerter}(k) = {}^Ev_k^T(H_I) \cdot \left\{ b\left[{}^Ea^D - {}^Ea^T(H_I)\right] \right\} \qquad \text{for } k = 1 \text{ to } 11, 23 \tag{A108}$$

where b is the constant of proportionality of the force generated by the inerter due to the relative acceleration between its two nodes and H_I is an arbitrary distance from the base of the tower. Gravitational force on the TMDI brings about generalised active forces as

$$F_k\Big|_{TMDI} = {}^Ev_k^D \cdot (-m_{TMDI}g\hat{z}_2) \tag{A109}$$

The elements of the system matrices can be obtained as

$$\{-f(\dot{q},q,t)\}\Big|_{TMDIGrav}(k) = {}^Ev_k^D \cdot (-m_{TMDI}g\hat{z}_2) \qquad \text{for } k,l = 1 \text{ to } 11, 23 \tag{A110}$$

The spring and the damper attached to the TMDI mass brings about generalised active force given as

$$\{-f(\dot{q},q,t)\}\Big|_{TMDIElastic}(k) = \frac{\partial V^{TMDI}}{\partial q_r} = -k_{TMDI}q_{TMDI} \qquad \text{for } k = 23 \tag{A111}$$

where V^{TMD} is the potential energy stored in the spring of the TMD. Using Rayleigh damping technique the damping is assumed to be proportional to the stiffness. The generalised active forces arising from the damping is given as

$$\{-f(\dot{q},q,t)\}\Big|_{TMDIDamp}(k) = -\frac{\zeta_{TMDI}k_{TMDI}}{\pi f_{TMDI}}\dot{q}_{TMDI} \tag{A112}$$

$$\text{for } k = 23$$

where m_{TMDI}, k_{TMDI}, f_{TMDI} and ζ_{TMDI} are the damper mass, stiffness, frequency of the TMDI in Hz and damping ratio respectively. Including these terms in the global system matrices of the wind turbine forms the final system matrices for a wind turbine with a TMDI installed in the nacelle.

Appendix E. Blade and Tower Deflection Shapes

Tower axial deflections deflection shape functions are given as [65]

$$S_{ij}^{TFA}(h) = \int_0^h \left[\frac{d\phi_i^{TFA}(h')}{dh'} \frac{d\phi_j^{TFA}(h')}{dh'} \right] \quad \text{for } i, j = 1, 2$$

$$S_{ij}^{TSS}(h) = \int_0^h \left[\frac{d\phi_i^{TSS}(h')}{dh'} \frac{d\phi_j^{TSS}(h')}{dh'} \right] \quad \text{for } i, j = 1, 2$$

where $S_{ij}^{TFA}(r)$ and $S_{ij}^{TSS}(r)$ are symmetric. Blade 1 axial deflections deflection shape functions are given as[65]

$$S_{ij}^{B1}(r) = \int_0^r \left[\frac{d\phi_i^{B1}(r)}{dr'} \frac{d\phi_j^{B1}(r)}{dr'} + \frac{d\psi_i^{B1}(r)}{dr'} \frac{d\psi_j^{B1}(r)}{dr'} \right] dr'$$

$$\text{for } i, j = 1, 2, 3$$

and $S_{ij}^{B1}(r) = S_{ji}^{B1}(r)$ (i.e., the shape functions are symmetric). In the above equation ϕ_1^{B1}, ϕ_2^{B1}, ϕ_3^{B1}, ψ_1^{B1}, ψ_2^{B1} and ψ_3^{B1} are the twisted mode shapes that can be obtained as [65]

$$\phi_1^{B1}(r) = \int_0^r \left\{ \int_0^{r'} \frac{d^2\phi_1^{B1F}(r'')}{dr''^2} \cos(\theta_s^{B1}(r'')) dr'' \right\} dr'$$

$$\phi_2^{B1}(r) = \int_0^r \left\{ \int_0^{r'} \frac{d^2\phi_2^{B1F}(r'')}{dr''^2} \cos(\theta_s^{B1}(r'')) dr'' \right\} dr'$$

$$\phi_3^{B1}(r) = \int_0^r \left\{ \int_0^{r'} \frac{d^2\phi_1^{B1E}(r'')}{dr''^2} \sin(\theta_s^{B1}(r'')) dr'' \right\} dr'$$

$$\psi_1^{B1}(r) = -\int_0^r \left\{ \int_0^{r'} \frac{d^2\phi_1^{B1F}(r'')}{dr''^2} \sin(\theta_s^{B1}(r'')) dr'' \right\} dr'$$

$$\psi_2^{B1}(r) = -\int_0^r \left\{ \int_0^{r'} \frac{d^2\phi_2^{B1F}(r'')}{dr''^2} \sin(\theta_s^{B1}(r'')) dr'' \right\} dr'$$

$$\psi_3^{B1}(r) = \int_0^r \left\{ \int_0^{r'} \frac{d^2\phi_1^{B1E}(r'')}{dr''^2} \cos(\theta_s^{B1}(r'')) dr'' \right\} dr'$$

Appendix F. Model Verification Results

The motion of the floating wind turbine platform is shown in Figure A1.
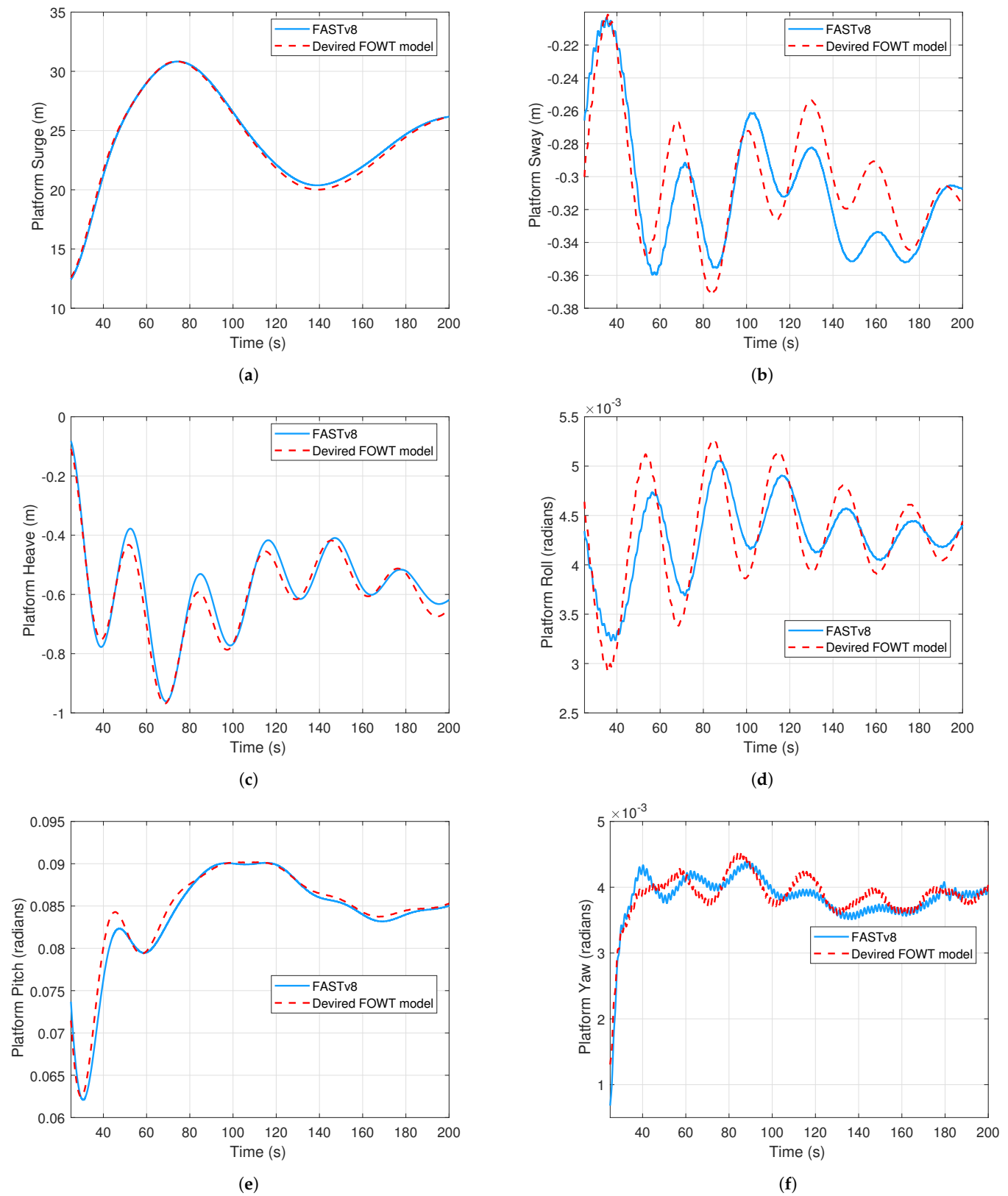
Figure A1. Model verification: motion of the floating offshore wind turbine platform. (**a**) Platform surge; (**b**) Platform sway; (**c**) Platform heave; (**d**) Platform roll; (**e**) Platform pitch; (**f**) Platform yaw.

References

1. Council, G. *Global Wind Report 2006*; Global Wind Energy Council: Brussels, Belgium, 2006.
2. Council, G. *Global Wind Report 2021*; Global Wind Energy Council: Brussels, Belgium, 2021.
3. Murtagh, P.; Basu, B.; Broderick, B. Along-wind response of a wind turbine tower with blade coupling subjected to rotationally sampled wind loading. *Eng. Struct.* **2005**, *27*, 1209–1219. [CrossRef]
4. Lackner, M.A.; Rotea, M.A. Passive structural control of offshore wind turbines. *Wind Energy* **2011**, *14*, 373–388. [CrossRef]
5. Basu, B.; Zhang, Z.; Nielsen, S.R. Damping of edgewise vibration in wind turbine blades by means of circular liquid dampers. *Wind Energy* **2016**, *19*, 213–226. [CrossRef]
6. Fitzgerald, B.; Basu, B.; Nielsen, S.R. Active tuned mass dampers for control of in-plane vibrations of wind turbine blades. *Struct. Control Health Monit.* **2013**, *20*, 1377–1396. [CrossRef]
7. Fitzgerald, B.; Basu, B. Cable connected active tuned mass dampers for control of in-plane vibrations of wind turbine blades. *J. Sound Vib.* **2014**, *333*, 5980–6004. [CrossRef]
8. Zhang, Z.; Basu, B.; Nielsen, S.R. Tuned liquid column dampers for mitigation of edgewise vibrations in rotating wind turbine blades. *Struct. Control Health Monit.* **2015**, *22*, 500–517. [CrossRef]
9. Fitzgerald, B.; Sarkar, S.; Staino, A. Improved reliability of wind turbine towers with active tuned mass dampers (ATMDs). *J. Sound Vib.* **2018**, *419*, 103–122. [CrossRef]
10. Zhang, Z.L.; Chen, J.B.; Li, J. Theoretical study and experimental verification of vibration control of offshore wind turbines by a ball vibration absorber. *Struct. Infrastruct. Eng.* **2014**, *10*, 1087–1100. [CrossRef]
11. Fitzgerald, B.; Basu, B. A monitoring system for wind turbines subjected to combined seismic and turbulent aerodynamic loads. *Struct. Monit. Maint.* **2017**, *4*, 175–194.
12. Cong, C. Stochastic Vibrations Control of Wind Turbine Blades Based on Wireless Sensor. *Wirel. Pers. Commun.* **2018**, *102*, 3503–3515. [CrossRef]
13. Fitzgerald, B.; Basu, B. Structural control of wind turbines with soil structure interaction included. *Eng. Struct.* **2016**, *111*, 131–151. [CrossRef]
14. Harte, M.; Basu, B.; Nielsen, S.R. Dynamic analysis of wind turbines including soil-structure interaction. *Eng. Struct.* **2012**, *45*, 509–518. [CrossRef]
15. Buckley, T.; Watson, P.; Cahill, P.; Jaksic, V.; Pakrashi, V. Mitigating the structural vibrations of wind turbines using tuned liquid column damper considering soil-structure interaction. *Renew. Energy* **2017**, *120*, 322–341. [CrossRef]
16. Achmus, M.; Kuo, Y.S.; Abdel-Rahman, K. Behavior of monopile foundations under cyclic lateral load. *Comput. Geotech.* **2009**, *36*, 725–735. [CrossRef]
17. Carswell, W.; Arwade, S.R.; DeGroot, D.J.; Lackner, M.A. Soil–structure reliability of offshore wind turbine monopile foundations. *Wind Energy* **2015**, *18*, 483–498. [CrossRef]
18. Dinh, V.N.; Basu, B. Impact of spar-nacelle-blade coupling on the edgewise response of floating offshore wind turbines. *Coupled Syst. Mech.* **2013**, *2*, 231–253. [CrossRef]
19. Lackner, M.A. Controlling platform motions and reducing blade loads for floating wind turbines. *Wind. Eng.* **2009**, *33*, 541–553. [CrossRef]
20. Lackner, M.A. An investigation of variable power collective pitch control for load mitigation of floating offshore wind turbines. *Wind Energy* **2013**, *16*, 519–528. [CrossRef]
21. Karimirad, M.; Moan, T. Wave-and wind-induced dynamic response of a spar-type offshore wind turbine. *J. Waterw. Port Coast. Ocean. Eng.* **2011**, *138*, 9–20. [CrossRef]
22. Waris, M.B.; Ishihara, T. Dynamic response analysis of floating offshore wind turbine with different types of heave plates and mooring systems by using a fully nonlinear model. *Coupled Syst. Mech.* **2012**, *1*, 247–268. [CrossRef]
23. Karimirad, M.; Moan, T. Stochastic dynamic response analysis of a tension leg spar-type offshore wind turbine. *Wind Energy* **2013**, *16*, 953–973. [CrossRef]
24. Wang, K.; Moan, T.; Hansen, M.O. Stochastic dynamic response analysis of a floating vertical-axis wind turbine with a semi-submersible floater. *Wind Energy* **2016**, *19*, 1853–1870. [CrossRef]
25. Jonkman, J.M.; Buhl, M.L., Jr. *Fast User's Guide—Updated August 2005*; Technical Report; National Renewable Energy Laboratory (NREL): Golden, CO, USA, 2005.
26. Jonkman, J.M. *Dynamics Modeling and Loads Analysis of an Offshore Floating Wind Turbine*; University of Colorado Boulder: Boulder, CO, USA, 2007.
27. Kane, T.R.; Levinson, D.A. *Dynamics, Theory and Applications*; McGraw Hill: New York, NY, USA, 1985.
28. Lee, D.; Hodges, D.H.; Patil, M.J. Multi-flexible-body Dynamic Analysis of Horizontal Axis Wind Turbines. *Wind Energy* **2002**, *5*, 281–300. [CrossRef]
29. Lee, D.; Hodges, D. *Multi-Flexible-Body Analysis for Applications to Wind Turbine Control Design*; School of Aerospace Engineering, Georgia Institute of Technology: Atlanta, GA, USA, 2003.
30. Sarkar, S.; Chen, L.; Fitzgerald, B.; Basu, B. Multi-resolution wavelet pitch controller for spar-type floating offshore wind turbines including wave-current interactions. *J. Sound Vib.* **2020**, *470*, 115170. [CrossRef]
31. Sarkar, S.; Fitzgerald, B. Vibration control of spar-type floating offshore wind turbine towers using a tuned mass-damper-inerter. *Struct. Control Health Monit.* **2020**, *27*, e2471. [CrossRef]

32. Sarkar, S.; Fitzgerald, B.; Basu, B. Individual blade pitch control of floating offshore wind turbines for load mitigation and power regulation. *IEEE Trans. Control Syst. Technol.* **2020**, *29*, 305–315. [CrossRef]
33. Sarkar, S.; Fitzgerald, B.; Basu, B. Nonlinear model predictive control to reduce pitch actuation of floating offshore wind turbines. *IFAC-PapersOnLine* **2020**, *53*, 12783–12788. [CrossRef]
34. Larsen, T.J.; Hansen, A.M. *How 2 HAWC2, The User'S Manual*; Risø National Laboratory: Roskilde, Denmark, 2007.
35. Stewart, G.; Muskulus, M. A review and comparison of floating offshore wind turbine model experiments. *Energy Procedia* **2016**, *94*, 227–231. [CrossRef]
36. Staino, A.; Basu, B.; Nielsen, S.R. Actuator control of edgewise vibrations in wind turbine blades. *J. Sound Vib.* **2012**, *331*, 1233–1256. [CrossRef]
37. Huang, N.E.; Chen, D.T.; Tung, C.C.; Smith, J.R. Interactions between steady won-uniform currents and gravity waves with applications for current measurements. *J. Phys. Oceanogr.* **1972**, *2*, 420–431. [CrossRef]
38. Tung, C.C.; Huang, N.E. Influence of current on statistical properties of waves. *J. Waterw. Harb. Coast. Eng. Div.* **1974**, *100*, 267–278. [CrossRef]
39. Thomas, G. Wave-current interactions: An experimental and numerical study. Part 1. Linear waves. *J. Fluid Mech.* **1981**, *110*, 457–474. [CrossRef]
40. Silva, M.; Vitola, M.; Esperança, P.; Sphaier, S.; Levi, C. Numerical simulations of wave–current flow in an ocean basin. *Appl. Ocean. Res.* **2016**, *61*, 32–41. [CrossRef]
41. Ismail, N.M. Wave-current models for design of marine structures. *J. Waterw. Port Coast. Ocean. Eng.* **1984**, *110*, 432–447. [CrossRef]
42. Hedges, T. Some effects of currents on wave spectra. In Proceedings of the First Indian Conference in Ocean Engineering, Madras, India, 18–20 February 1981; Volume 1, pp. 30–35.
43. Hedges, T.S.; Anastasiou, K.; Gabriel, D. Interaction of random waves and currents. *J. Waterw. Port Coast. Ocean. Eng.* **1985**, *111*, 275–288. [CrossRef]
44. Phillips, O.M. *The Dynamics of the Upper Ocean*; CUP Archive: Cambridge, UK, 1966.
45. Azcona, J.; Palacio, D.; Munduate, X.; González, L.; Nygaard, T.A. Impact of mooring lines dynamics on the fatigue and ultimate loads of three offshore floating wind turbines computed with IEC 61400-3 guideline. *Wind Energy* **2017**, *20*, 797–813. [CrossRef]
46. Jonkman, B.J. *TurbSim User'S Guide: Version 1.50*; Technical Report; National Renewable Energy Lab (NREL): Golden, CO, USA, 2009.
47. Burton, T.; Jenkins, N.; Sharpe, D.; Bossanyi, E. *Wind Energy Handbook*; John Wiley & Sons: Hoboken, NJ, USA, 2011.
48. Moriarty, P.J.; Hansen, A.C. *AeroDyn Theory Manual*; Technical Report; National Renewable Energy Lab.: Golden, CO, USA, 2005.
49. Hansen, M.O. *Aerodynamics of Wind Turbines*; Routledge: Oxfordshire, UK, 2015.
50. Ning, S.A. A simple solution method for the blade element momentum equations with guaranteed convergence. *Wind Energy* **2014**, *17*, 1327–1345.
51. Ning, A.; Hayman, G.; Damiani, R.; Jonkman, J.M. Development and Validation of a New Blade Element Momentum Skewed-Wake Model within AeroDyn. In Proceedings of the 33rd Wind Energy Symposium, Kissimmee, FL, USA, 5–9 January 2015; p. 0215.
52. Chen, L.; Basu, B.; Nielsen, S.R. A coupled finite difference mooring dynamics model for floating offshore wind turbine analysis. *Ocean. Eng.* **2018**, *162*, 304–315. [CrossRef]
53. Tjavaras, A.A. The Dynamics of Highly Extensible Cables. Ph.D. Thesis, Massachusetts Institute of Technology, Cambridge, MA, USA, 1996.
54. Tjavaras, A.; Zhu, Q.; Liu, Y.; Triantafyllou, M.; Yue, D. The mechanics of highly-extensible cables. *J. Sound Vib.* **1998**, *213*, 709–737. [CrossRef]
55. Gobat, J.; Grosenbaugh, M. Time-domain numerical simulation of ocean cable structures. *Ocean. Eng.* **2006**, *33*, 1373–1400. [CrossRef]
56. Fitzgerald, B.; Basu, B. Vibration control of wind turbines: recent advances and emerging trends. *Int. J. Sustain. Mater. Struct. Syst.* **2020**, *4*, 347–372. [CrossRef]
57. Zhang, Z.; Fitzgerald, B. Tuned mass-damper-inerter (TMDI) for suppressing edgewise vibrations of wind turbine blades. *Eng. Struct.* **2020**, *221*, 110928. [CrossRef]
58. Marian, L.; Giaralis, A. Optimal design of a novel tuned mass-damper–inerter (TMDI) passive vibration control configuration for stochastically support-excited structural systems. *Probabilistic Eng. Mech.* **2014**, *38*, 156–164. [CrossRef]
59. Giaralis, A.; Petrini, F. Wind-induced vibration mitigation in tall buildings using the tuned mass-damper-inerter. *J. Struct. Eng.* **2017**, *143*, 04017127. [CrossRef]
60. Jonkman, J.M.; Butterfield, S.; Musial, W.; Scott, G. *Definition of a 5-MW Reference Wind Turbine for Offshore System Development*; National Renewable Energy Laboratory: Golden, CO, USA, 2009.
61. Das, S.; Mohamed Sajeer, M.; Chakraborty, A.; Sarkar, S. Shape memory alloy-based centrifugal stiffening for response reduction of horizontal axis wind turbine blade. *Struct. Control Health Monit.* **2021**, *28*, e2669. [CrossRef]
62. Mitra, A.; Sarkar, S.; Chakraborty, A.; Das, S. Sway vibration control of floating horizontal axis wind turbine by modified spar-torus combination. *Ocean Eng.* **2021**, *219*, 108232. [CrossRef]

63. Fitzgerald, B.; Igoe, D.; Sarkar, S. A Comparison of Soil Structure Interaction Models for Dynamic Analysis of Offshore Wind Turbines. J. Phys. Conf. Ser. **2020**, *1618*, 052043. [CrossRef]

64. Kane, T.; Ryan, R.; Banerjee, A. Dynamics of a cantilever beam attached to a moving base. *J. Guid. Control Dyn.* **1987**, *10*, 139–151. [CrossRef]

65. Jonkman, J.M. *Modeling of the UAE Wind Turbine for Refinement of FAST_AD*; Technical Report; Citeseer: University Park, PA, USA, 2003.